

## AC Loss in Nb<sub>3</sub>Sn Superconducting Cable - Mechanisms and Measurement

John D. Larson III, Roger Mitchell\*,  
Jeremy A. Good\*, Jose Lopez\*\*  
Analytical/Medical Laboratory  
HPL-95-119  
September, 1995

superconductors,  
AC resistance,  
transport current

The AC dissipation of Nb<sub>3</sub>Sn superconducting cable, formed in a Maxwell pair circuit configuration and operated at temperatures of 8° K or 12° K, is measured. The circuit is driven by an AC current, ranging in frequency from 10 Hz to 10 kHz, and at selected peak amplitudes up to 50 Amperes. The test circuit reactance, dissipated power, and drive current are the measured data. Combining these into a complex impedance Z, the resistive part ( $R_{ac} \sim 1\mu\text{Ohm}$ ) is found to be quite small compared to the inductive part ( $\omega L \sim 1 \text{ milliOhm}$ ), which makes  $R_{ac}$  difficult to measure with conventional impedance meters.

A new calorimetric measurement technique, sensitive primarily to the resistive loss, is described. Precision phase angle measurements, critical lead placement, and inductive compensation are thus eliminated. The calorimeter measures dissipated AC power in the Maxwell pair, by substitution of DC power in two nearby auxiliary heater coils. The accuracy is set by the system stability, typically  $\frac{\Delta P}{P} \sim \pm 1\%$ , during an experiment.

Several superconducting cables were measured. The result is data for the equivalent series resistance  $R_{ac}$  vs. frequency. In addition, the effect of AC drive current amplitude, operating temperature, and applied magnetic flux intensity  $B_0$  on  $R_{ac}$ , is experimentally evaluated.

A simplified theory of AC loss mechanisms in superconductors is developed. Two mechanisms, hysteresis loss in the superconductor and inductive-Ohmic loss in the metal jacketing, account for the observed resistance  $R_{ac}$ . A series resistance  $R_H$ , increasing linearly with frequency, and a shunt conductance G, emerge from the theory as good descriptors of the measured data.

\* *Cryogenic, Ltd.*, London, England.

\*\* *Universidad Politecnica of Madrid*, Madrid, Spain. Jose Lopez worked as a EuroStudent for HP Laboratories, 1994.

# "AC Loss in Nb<sub>3</sub>Sn Superconducting Cable - Mechanisms and Measurements "

## **1 Introduction**

### **1.1 AC Losses in Superconductors**

For real time Magnetic Resonance Imaging (MRI) applications, the concept of using superconducting gradient coils is introduced in this work. A major problem encountered in designing such coils is a paucity of data on the AC resistance of commercially available superconducting cable. Obtaining and reporting engineering data at frequencies up to 10 kilohertz and at high current levels on candidate superconducting cables, is the motivation for this work.

In this paper, the transport current AC resistance of a few types of commercially available Nb<sub>3</sub>Sn superconducting cable is measured calorimetrically. A new calorimeter is described which is sensitive mainly to resistive loss and insensitive to the reactive power, thus eliminating the precision determination of phase angle and the critical lead placement required in impedance techniques. Measurements of dissipated power are made as a function of frequency, current amplitude, applied DC magnetic field, and temperature.

A simplified theory of AC loss in superconducting cable is presented as a guide to interpreting the data. The power dissipation can be interpreted as arising due to 1) hysteresis mechanisms in the superconductor, and 2) Ohmic losses in the normal metal cladding. Two coefficients -  $R_{H0}$  and G, along with the inductance L - are found to describe the sources of power dissipation adequately.

### **1.2 Superconducting Gradient Coils in MRI**

In a conventional whole body MRI machine<sup>1,2</sup>, gradients in the polarizing magnetic field are used to obtain spatial resolution in the tissue imaged. The gradients are produced by coils placed in the warm bore of the magnet. The typical gradient coil set produces linear magnetic field gradients  $G_i = \frac{\partial B_z}{\partial x_i}$  in the  $i = x, y,$  or  $z$  direction (by convention the z-axis aligns with the polarizing field  $B_0$ ). To accommodate the largest expected patients, the gradients fields must be applied over a cylindrical space of  $\sim 60$  cm diameter by  $\sim 40$  cm in the z direction. In "real time" pulse sequences such as echo planar imaging<sup>3,4</sup> (EPI), the gradients  $G_i$  are applied sequentially in time, are oscillated at frequencies ranging up to several hundred Hz, and at least one axis must be capable of producing gradient waveforms with amplitude  $\sim 20$  milliTesla/m and rise times  $\sim 50$  microseconds. To achieve such amplitudes and rise times with typical whole body MRI coils, the output amplifier must produce a drive voltage of several hundred volts, followed by a low sustaining voltage to maintain currents of several hundred Amperes. The waveforms are tightly controlled as to amplitude, shape, and repetition rate. The waveshapes are unique to each pulse sequence<sup>5</sup> application, are typically variants on a trapezoidal wave for EPI or a chirped sine wave<sup>6</sup> for spiral imaging, and all have fundamental frequencies in the audio range. As the imaging system resolution increases (image pixel becomes smaller), or the temporal resolution (speed) increases, the gradient amplitude and frequency of at least one component  $G_i$ , will increase.

Typical external, warm bore gradient coils are fabricated from high conductivity copper. For the high resolution/high speed gradient component  $G_i$  sketched above, peak power dissipation of up to 50 to 100 kW can

be expected in a whole body MRI machine. Such coils also produce intense audio sound levels, which is a drawback and a safety factor in imaging patients.

Alternatively, if the gradient coils could be made from a superconductor and placed inside the magnet cryostat, much lower power dissipation would be expected to occur, due to the extremely low (but non-zero) AC resistance of superconductors. There is data available<sup>7</sup> on the power dissipation at high drive current levels in some types of superconductor, but it is obtained only at isolated frequencies, such as 50 Hz or 60 Hz. Likewise, the gradient coil noise typically associated with MRI scanners would be greatly attenuated by the vacuum environment of the cryostat.

### 1.3 Pulse Sequences, Power Dissipation, and Cryocoolers

Although superconductors exhibit no power dissipation to steady DC currents<sup>8</sup>, alternating current (AC) does produce a small power dissipation<sup>9,10,11,12</sup>. In an MRI application, high transition temperature Nb<sub>3</sub>Sn or Nb<sub>3</sub>Ge superconducting cable would be used to form the gradient coil windings, and would be within the cryogenic temperature/vacuum space. It is further envisaged to use a cryocooler refrigerator to maintain the cryogenic operating temperature (~ 10<sup>0</sup> K). One presently advertised, commercially available cryocooler<sup>13</sup> can provide ~10 Watts maximum cooling capacity at 11<sup>0</sup> K. Thus, a gradient coil playing out the most extreme MRI pulse sequence, would be limited to 2 to 3 Watts dissipation in order to avoid overloading the cryocooler.

The most demanding pulse sequences for real time MRI are those which capture a full frame of image data in one excitation, for example, single shot echo planar sequences running at 100 milliseconds acquisition time (10 frames/sec), a 128 x 128 sampling of k-space, and a 25.6 cm Field of View (2 mm resolution, in-plane). The required READ gradient is played out in a trapezoidal waveform of rise/fall time ~ 50 μs, period of 1563 μs, and flat top amplitude of +/- 17 mT/m. This corresponds to a waveform with fundamental frequency of 640 Hz, and significant energy up to the 8<sup>th</sup> harmonic. Appendix A shows further details of the sequence, and the harmonic content of the waveform.

As an example of the problem, if a simple (but non-optimum) Maxwell pair gradient coil<sup>14</sup> design is used to generate the gradient field, a drive current of ~ 1300 Amps is required to achieve the above gradient amplitude. To hold power dissipation below 2 Watts, the effective resistance presented by the Maxwell pair gradient coil set must be ~ 1 μOhm. Optimization of the gradient coils<sup>15,16,17</sup> will decrease the required drive current, which will increase the allowable resistance, but the order of magnitude will be in the 1 to 100 μOhm range.

## 2 Theory of AC Losses in Superconductors

### 2.1 Overview

Current is carried in superconductors, as in other materials, by electrons. Below the critical temperature the material becomes superconducting, because electrons are condensed into the superconducting state, in which two electrons form Cooper pairs<sup>8,9,18</sup> by phonon interaction through the lattice of the crystal structure.

Cooper pairs have the property that once accelerated into motion, they continue to move through the lattice without scattering, i.e. no loss of energy. By contrast the normal electrons in a metal which move independently through the lattice do scatter off lattice imperfections and phonons, losing energy which must be replaced by maintaining an electric field in the conductor; hence power is dissipated.

At absolute zero all the conduction electrons are superconducting, but at practical temperatures there are also normal electrons which have not changed to the superconducting state. As a result, if an electric field is applied to a superconductor to maintain an AC current flow, some power dissipation can be expected on this account alone.

In the absence of magnetic fields the power dissipation is very small and for this reason, cavities of niobium and other superconductors are used successfully to generate Q's in excess of  $10^7$ . The position is however quite different in the presence of strong magnetic fields or large transport currents, where the self field of the current is significant.

A superconductor cooled in a magnetic field will, if the field is below a critical value, expel the magnetic field as it changes to the superconducting state. This is known as the Meissner effect. A shielding current is set up in the surface of the conductor.

If the field is increased above a certain critical value, the energy required to maintain the expulsion of the field is too great and the material switches back from the superconducting state to the normal state.

All the common elemental superconductors except niobium show this type of behavior and have critical fields of a few hundred Oersteds. This makes these materials only suitable for low field and small signal applications such as electromagnetic shielding, resonant cavities and devices such as SQUIDS. They are known as type I superconductors. A second class of type II superconductors which are mostly alloys and compounds, exhibit a different behavior in magnetic field. Above a lower critical field, typically some 50 Oersted ( $\mu_0 H = 0.005$  Tesla), the superconductor permits field to enter and forms a mixed state of normal vortices or fluxoids<sup>18</sup>. Each fluxoid contains one unit of flux ( $\phi_0 \sim 2 \times 10^{-15}$  Weber), which corresponds to one Cooper pair orbiting the fluxoid. At the center of the fluxoid there is a normal core where the superconducting state disappears and there are normal electrons. Moving out from the core the proportion of superconducting electrons rises towards its full value. At its center the core contains a strong magnetic field which is surrounded by a screening current. As the external magnetic field is increased, more fluxoids are created at the surface of the material and move into the body of the superconductor. The density of fluxoids is directly proportional to the field,  $N\phi_0 = B$ , within the superconductor. Eventually a field is reached at which the fluxoids are packed so close together that the normal cores overlap and at this point (the upper critical field) the superconducting state is extinguished.

The upper critical field can be very high, up to 10 Tesla for NbTi or 24 Tesla for Nb<sub>3</sub>Sn. It is very important to note that this mixed state does not imply any ability to carry transport current without loss. Ideal alloys or samples of pure niobium show ideal type II behavior. Fluxoids enter and leave the superconductor reversibly and without hysteresis. This reversible behavior is only achieved if there are no lattice or surface imperfections which can form pinning sites for the fluxoids. Such materials are known as soft superconductors and the same considerations apply to both type I and type II superconductors. Only ideal or soft superconductors can be made to demonstrate the Meissner effect which relies on reversibility and demonstrates the thermodynamic properties of the superconducting phenomena.

If a type II superconductor is work hardened or made to have short range variations in its crystal structure by any means such as inclusions or grain boundaries, then fluxoids will be trapped and only move irreversibly. In particular, variations in the density of fluxoids within the superconductor become possible and this variation in density represents a variation in the flux density or local magnetic field. Gradients of fluxoid density correspond to transport currents within the body of a conductor. In the simplest geometry, consider a thin sheet of superconductor with a strong field parallel to one surface of the superconductor. The fluxoids will penetrate this surface but as they move from the surface, some will be pinned, leading to a gradient of fluxoid (and flux) density. At a finite distance depending on the fluxoid density gradient achieved, the density of fluxoids will reach zero and the magnetic field will be zero. This corresponds to, and is identically equivalent to a macroscopic transport current flowing in the plane of the superconductor perpendicular to the field direction. A high gradient of fluxoid density corresponds to a high current density and, for practical superconductors, great efforts are made to achieve the highest gradients with the strongest pinning effects. The effect of hardening the superconductor is dramatic. Pure single crystal niobium in low fields, has been reported with critical currents of  $10 \text{ Amp/cm}^2$ , while high current Niobium based superconductors can achieve  $10^8 \text{ Amps/cm}^2$  under the same conditions.

If the external field and the surface of the conductor is reversed, all the fluxoids that are present will be first extracted and replaced by the same pattern of fluxoids pointing in the opposite direction. This is an irreversible process and leads to work being done by the external field on the superconductor. This work appears as heating of the conductor.

Even if the external field is just reduced to zero, fluxoids will be extracted but only so as to reduce the density on the surface to zero. Within the body of the superconductor the density of fluxoids will rise at the critical gradient to half the depth to which the original field penetrated, and then fall again to zero. These fluxoids represent the trapped flux.

The work done in driving the fluxoids into the superconductor is the product of the distance the fluxoids move and the force required to drive them past the pinning centers. The latter is proportional to the critical gradient permitted, i.e. the current density of the material. To obtain a large total current the volume of the conductor must be increased, so increasing the depth of flux penetration and the work done. It can be reduced by keeping the thickness of conductors and depth of the penetration to the minimum possible.

In practical conductors this is achieved by having continuous filaments of superconductor embedded in a matrix of normal metal. Even for quasi DC applications this has the practical benefit that during energization of a current in a solenoid, the dissipation is reduced and the tendency for uncontrolled flux penetration, known as a flux jump, is reduced leading to more reliable coil operation. For DC applications the matrix may be copper and the superconducting filaments, which are typically 50 micron diameter of NbTi, may be co-drawn into a wire. For AC applications far finer filaments are produced surrounded by a resistive matrix. To provide for equal current sharing between the filaments and to limit flux linkage between the filaments the whole conductor is twisted along its axis with a pitch of 25-50 mm.

In our application with operation envisaged above 4.2° K, the ideal candidate conductor that is in commercial production is Nb<sub>3</sub>Sn produced by the bronze route. In this process Nb filaments, up to 10,000 in number and of 3-5 micron diameter, are drawn in a copper-tin bronze matrix. On heat treating at 700°C, some of the tin diffuses into the Nb to create the Nb<sub>3</sub>Sn intermetallic superconductor which has very high current capacity and remains superconducting to 17° K.

## 2.2 Loss Mechanisms

The loss mechanisms under AC conditions in these conductors have several sources. Firstly, at low frequencies there is the requirement to drive flux in and out of the superconductor during each AC cycle. This is termed a hysteresis loss, where a certain amount of energy on each AC cycle is required to move the flux in or out. The power loss is proportional to the rate at which this occurs, thus the losses will be proportional to frequency to the first power and to the AC field or current to a higher power, since higher fields and currents require more flux to penetrate further into each superconductor filament of conductor during each AC cycle. Figure 1 illustrates how increasing the magnetic field increases the penetration of flux into the superconductor. For small values of magnetic field relative to the critical field, one expects the power dissipation to be proportional to AC transport current squared, increasing to current to the fourth, sixth, etc. at higher drive levels.

Secondly, with finite inductance there is a finite voltage established along the conductor leading to a drive voltage on the normal electrons in the matrix. This inductive voltage increases with frequency, and the associated power dissipation increases as frequency squared.

Related to this is the fact that as the filaments are twisted to ensure equal current distribution, there is finite loop area between them for all directions of magnetic field. Consider applying an AC field perpendicular to a conductor containing just two filaments in a normal matrix, as in Figure 2. Currents are induced in the two filaments around each loop area and the currents transfer between the filaments at the crossover points through the matrix. These losses will increase with frequency squared and are proportional to the size of the loop area

which suggests using smaller conductors. The losses also increase as the conductivity of the matrix increases. The proximity of adjacent filaments in the superconductor is important, and is controlled by wire diameter and twist pitch. If the diameter of a filament is decreased while at the same time increasing the number of filaments to maintain a constant amount of superconductor, the filaments will be closer together leading to more current passing through the matrix. Twist pitch is also clearly an important factor, as it also controls the amount of loop area .

Three frequency regimes can then be clarified for a superconductor carrying a transport current in a magnetic field. At DC or very low frequency the losses are zero or negligible. At low frequencies the superconducting hysteretic effects dominate, and at higher frequencies the normal resistivity effects which are proportional to  $f^2$ , are dominant.

### 2.3 Loss Mechanisms - Equivalent Circuit for a Maxwell Pair

It is desired to evaluate the loss in a manner generally applicable to a wide variety of superconducting devices carrying transport current, and it is also desired to apply the results to a MRI gradient coil situation. A Maxwell pair, as illustrated in Figure 3, is chosen as the structure to be evaluated. Although not an optimum gradient coil, a Maxwell pair is a good MRI prototype. It produces a linear gradient  $G_z$  in the z-directed field component over a reasonable distance, is easily fabricated, and is relatively easy to analyze. The Maxwell pair is assumed to be fabricated from superconducting cable, to be placed in a suitable cryogenic environment, and to have suitable current leads communicating to an outside current source at room temperature.

An equivalent electrical circuit, shown in Figure 4, can be used to represent the coil set. At the electrical terminals the coil set will appear as a net inductance (sum of the self inductance of each coil and the interconnect inductance, minus the mutual inductance between coils), plus a very small resistance which is frequency dependent, and a shunt conductance. The self inductance can be further broken into 1) the external inductance due to the magnetic field energy stored in the volume outside the cable and 2) the internal inductance due to the magnetic flux within the cable. The resistance arises from hysteresis loss in the superconductor. The shunt conductance arises from the normal electron current flowing in the matrix and metal jacket.

Melville<sup>10,11</sup> and Good<sup>18</sup> point out that the loss in superconducting filaments is quite dependent on the amplitude of the AC magnetic field, to a smaller extent the DC magnetic field present, the transport current, and the temperature. The magnetic fields can be either externally applied, or the field due to transport current flowing in the conductor. Non-linear effects are expected. All of these effects were observed in the cable tested.

The *DC regime* is the essentially lossless mode, where only joints in the superconducting cable contribute to the resistance. This loss mechanism is modeled as a **resistance  $R_{Series}$** , independent of frequency.

In the *low frequency* range, the losses are caused by flux trapping from the pinning sites purposely introduced into the superconductor to increase its current carrying capacity. The superconductor exhibits a B vs H relationship with **hysteresis**, which leads to the dissipation of energy each time H is changed. Appendix B discusses hysteresis in superconductors, and presents a simplified circuit model which shows power dissipation rising linearly with driving frequency  $f$ . Since the hysteresis loss in the superconductor depends on the details of the B vs H relationship, which is highly field and temperature dependent, one would expect strong non-linearities and temperature dependence to be observed in the AC losses arising from this process. The loss mechanism is modeled by a **resistance  $R_H$**  which increases linearly with frequency  $f$ :

$$R_H = R_{H0} \cdot f \quad (1)$$

At *higher frequencies*, the **inductive-Ohmic loss** of the normal metal jacket dominates. Referring again to the circuit model in Figure 4, an AC current I passing through the inductors causes a voltage  $V_L$ , proportional to

the time rate of change of the current, to appear across the inductance. From the equivalent circuit of Figure 4, the inductive voltage  $V_L$  is:

$$V_L = (R_H + j\omega L) \cdot I \quad (2)$$

where

$$L = L_{ext} + L_{int}$$

is the inductance of the coil set, and  $\omega$  is the radian frequency of the AC current.

A **shunt conductance**  $G$  is used to model the inductive-Ohmic loss. The inductive voltage  $V_L$  causes an in-phase current  $I_g$  to flow in  $G$ :

$$I_g = G \cdot V_L \quad (3)$$

(Note: all voltages and currents are taken to be peak values)

which results in electrical power, proportional to  $real(\frac{1}{2} \cdot V_L \cdot I_g^*)$ , to be dissipated in the conductance  $G$ . In a regime where the inductance dominates the circuit, the inductive-Ohmic power dissipation increase as  $f^2$  and determines the loss. Since the dissipation arises from conventional Ohmic losses in the normal metal jacket, one would not expect  $G$  to exhibit strong non-linear effects, temperature dependence, or to be strongly affected by external magnetic fields.

Finally, the inductance  $L$  is an important **parameter** to determining the loss, either through the internal inductance and the hysteresis component, or through the total inductance and the inductive-Ohmic loss mechanism. Inductances of the order 1 to 10 microHenry are typical of the test gradient coil sets envisaged, and can lead to the measurement difficulties discussed below.

## 2.4 Measurement Model - Maxwell Pair Coil Set

For a useful superconductor working in the audio frequency range, the discussion in section 1 showed that the target circuit resistance in a superconducting test gradient coil assembly had to be  $\sim 1 \mu\text{Ohm}$ , and the associated inductances of  $\sim 1$  microHenry would produce reactances of  $\sim 1000 \mu\text{Ohm}$ . Thus, a measurement extremely sensitive to the real part of the impedance is required. One could chose a straightforward measurement of the complex impedance  $Z = R + jX$ , e.g. with a Hewlett-Packard 4284A LCR Meter, as a means to measure the resistive loss  $R$ . To achieve an accuracy of  $\pm 10\%$  in  $R$ , the phase angle ( $89.943^\circ$  in this example) would have to be measured to an accuracy of  $\pm 0.007\%$ ! This is a difficult measurement<sup>19</sup> to make.

A better strategy is to choose a measurement scheme which is sensitive only to the power dissipated, not to the reactive power circulating in the coils. A calorimetric method is chosen, in which only the heat generated by the resistive portion of the current flowing in the test portion (the gradient coil set) will be detected. The experimental apparatus is a *calorimeter*, which is shown schematically in Figure 5. It is basically a closed system in which the heat in-flow and out-flow can be controlled and measured. By dissipating a measured amount of power in a heater within the calorimeter, and regulating the power input to hold a desired temperature  $T$ , one can use substitution methods to measure the unknown amount of power dissipated in the gradient coil under test. Now, the accuracy of determining the real part of impedance,  $R$ , is as accurate as the stability of the calorimeter to thermal leakage, and to the accuracy of measuring DC electric power.

A Maxwell pair gradient coil set of radius  $a = 0.05$  meters, coil spacing 0.09 meters is chosen as the test measurement vehicle. This amounts to a 1/7 scale model of a coil large enough for whole body MRI. A scale model coil was chosen to minimize apparatus cost, liquid helium consumption, thermal response time, and driver amplifier cost. Appendix C provides the system details, defines the circuit elements, and relates the measured power dissipation to the AC resistance of the superconductor. Appendix D details the apparatus.

## 2.5 Measurement Methodology

Referring again to Figure 5, a thermally closed, vacuum tight vessel contains the gradient coil set under test, a non-inductive heater, and a temperature sensor near the gradient coil. The apparatus has a thermal resistance linking the gradient coil at the desired temperature  $T$ , to a liquid helium reservoir at temperature  $T_0 = 4.2^\circ \text{K}$ . Normally, a copper wire is used as the link. In situations where higher power dissipation is experienced, helium transfer gas can be admitted to the vessel to increase the cooling rate. This increases the power required to maintain a given temperature.

An AC current of frequency  $f$  (radian frequency  $\omega = 2\pi f$ ) and amplitude  $I_p$  can be fed into the gradient coil set. A DC current of amplitude  $I_{\text{heater}}$  can be applied to the heater. A Conductus LTC-10 controller monitors the temperature and regulates the DC current to maintain the system temperature at a desired set point value  $T$ , for example,  $8^\circ \text{K}$ .

In operation, the experiment begins by cooling the apparatus to liquid helium temperature. A DC current,  $I_{\text{heater}}$ , is fed into the heaters and regulated to obtain a desired temperature  $T$ , within a defined error band  $\Delta T \sim \pm 0.001^\circ \text{K}$ . This amounts to reaching an equilibrium between the input heater power and the output power carried away by the thermal link or transfer gas. When thermal equilibrium is reached, the DC equilibrium heater voltage  $V_{h0}$  across the heaters, and the equilibrium heater current  $I_{h0}$ , are measured and stored. The power is computed as  $V_{h0} I_{h0}$ , and recorded as  $P_{\text{equilibrium}} = P_0$ . Typically, with the thermal time constant of the system and the stringent equilibrium condition imposed on  $\Delta T$ , it takes anywhere from 3 minutes to half an hour to reach equilibrium.

When the apparatus is at equilibrium, the stimulus AC current  $I_p(\omega)$  is fed into the gradient set. The additional power dissipated in the gradient coil set causes the temperature to rise. The feedback controller reduces the DC heater current until the temperature falls back toward the set point value  $T$ , continuing the process until thermal equilibrium is again achieved, or the heater power drops to zero and terminates the experiment. At equilibrium, the heater voltage  $V_h$  and heater current  $I_h$  are again recorded, and the heater power  $P_h = V_h I_h$  is calculated.

Under the assumption the gradient coils and the heater coils have the same thermal resistance to thermal ground ( $4.2^\circ \text{K}$ ), the power actually dissipated in the gradient coil is:  $P_{\text{diss}} = (P_0 - P_h)$ . This is equivalent to assuming that thermal equilibrium can only be maintained if one unit of power dissipated in the gradient coil is balanced by subtracting one unit of power from the heater coil. In practice, this assumption can be tested by using two heater coils, one in place of the gradient coil, to calibrate the apparatus. It turns out to be correct to within a few % in the case with vacuum in the inner container and only the copper wire as the thermal link, and not more than 30% off in the worst case with helium transfer gas in the apparatus. This systematic error is corrected out in the data reduction.

In the calorimetric measurement, the baseline value  $P_0$  is determined at one point in time, then the measurements of  $P_h(\omega)$  at various frequencies, ranging from 10 Hz to 10 kHz, are made sequentially over a time period of  $\sim 1$  hour. Baseline variation due mainly to control system noise, thermometer drift, and instrument error, is the single largest contributor to measurement error. By running the system over a period of  $\sim 1$  hour with no AC input to the coil set, the baseline power stability was determined to be  $\frac{\Delta P}{P} \sim \pm 1\%$  to hold a constant  $8^\circ \text{K}$  temperature. During data acquisition, data averaging is employed to reduce noise, and a standard deviation threshold in both power and temperature must be met before the point is accepted.

Appendix D contains drawings and photographs of the apparatus.

An automated data acquisition system was built to obtain the data. It employed an H-P Vectra computer running a LabVIEW<sup>(registered)</sup> software and hardware data acquisition package. A custom interface was built to acquire the heater voltages and currents. A full description is given in<sup>20</sup>.

## 2.6 Measurements

Referring again to the equivalent circuit model Figure 4, the voltage  $V_p$  across the terminals of the coil set within the vacuum/cryogenic space, is sensed by special leads which are brought out to a digital voltmeter (H-P 34401A). The current  $I_p$  is generated by a synthesized signal generator (H-P 3325B), amplified up to a selected value in the range of 10 to 90 Amps by a linear, bipolar power amplifier (Techron model HP7792), and sensed within the power amplifier by an current monitor. The LabVIEW system automatically adjusts the current amplitude until the set point value is achieved within  $\pm 0.25\%$ . From the ratio  $|V_p/I_p|$  which is calculated in software, the magnitude of the coil set impedance  $|Z|$  is obtained. The inductance  $L$  dominates the circuit, so the relation  $|Z| = \omega L$  can be used to accurately obtain the inductance.

To present the results of the measurements and emphasize the linear nature of the coil set, the *series equivalent AC resistance* of the coil set is calculated from the measured data,  $P_{diss}$  and the drive current  $I_p$  as:

$$R_{ac} = (2 \cdot P_{diss})/|I_p|^2 \quad (4)$$

As derived in Appendix C, the measured value  $R_{ac}$  can be related to the circuit parameters as:

$$R_{ac} = R_{Series} + R_H + R_G \quad (5)$$

where

$$R_G = (\omega L)^2 \cdot G$$

or since  $|Z| = \omega L$ , (5) could be re-arranged to read:

$$R_{ac} = R_{Series} + (R_{H0} \cdot f) + G \cdot |Z|^2 \quad (6)$$

which brings the measured quantities  $L$ ,  $R_{ac}$ , and  $f$  into an equation for the unknown parameters  $R_{Series}$ ,  $R_{H0}$ , and  $G$ .

The main error in  $R_{ac}$  is due to the baseline drift,  $\Delta P$ , and is  $\Delta R_{ac} = 2\Delta P/|I_p|^2$ ,  $\sim 0.1 \mu\text{Ohm}$  at  $I_p \sim 40$  Amps.

## 3 Experimental Results

In this set of experiments, Niobium-Tin ( $\text{Nb}_3\text{Sn}$ ) alloy superconductor based cable, is to be evaluated. Three different superconducting cable samples, of a filamentary design thought to produce low AC loss, were obtained from Vacuumschmelze GmbH, Hanua, Germany. These were formed into  $\pm 1$  turn or  $\pm 4$  turn, 100 mm diameter Maxwell pairs on a stainless steel mandrel, reacted in an oven to form the desired  $\text{Nb}_3\text{Sn}$  alloy, and then mounted in the measurement apparatus described in Appendix D.

The first type cable is Vacryflux NS 4500, non-stabilized superconductor with a bronze metal jacket and 0.4 mm in diameter. It is a 15 year old sample, composed of 4500 superconducting filaments, each in the range 4 to 6  $\mu\text{m}$  in diameter. It is referred to as: old, 0.4 mm wire.

The second type is a more modern version, Vacryflux HSNT 5185. It has 5185 filaments, in a bronze matrix, and is also 0.4 mm in diameter. It is referred to as: new, 0.4 mm wire.

The third type is a larger cross-section cable, Vacryflux HSNT 10000 TaI. It is included to test whether increasing the wire cross-sectional area decreases the loss resistance. It has 9690 filaments, each of 4.8  $\mu\text{m}$  diameter. The cable is 1.1 mm in diameter overall, and has a very large copper inner core. It is referred to as: 1.1 mm diameter wire.

A common method of decreasing loss is to parallel wires. A Rutherford cable was made to test the idea of lowering loss and increasing current carrying capacity by using multiple strands. It is made as follows: a copper/nickel wire 0.6 mm in diameter was used as a base on which to twist 6 strands of the new, 0.4 mm wire cable, with a 13 mm twist pitch. This cable was further formed into the 100 mm diameter,  $\pm 1$  turn Maxwell

pair coil, and reacted. In a final step the coil was slipped off the mandrel and mounted into the experimental apparatus.

The AC impedance was measured versus frequency and drive current amplitude. Temperature, background magnetic field, and number of turns were important parameters which could be varied. Since inductance is a key parameter, the measured inductance of various coils will be presented first.

### 3.1 Measured Inductance

The inductance is easily determined from the measured magnitude of the impedance  $|Z|$ . In Figure 6 is shown the  $|Z|$  data for a 4 turn coil set, 0.4 mm diameter wire, with a single pair of interconnect wires. The inductance measured is 8.16 microHenry, while the predicted value from Appendix C is 8.88 microHenry.

For a  $\pm 1$  turn coil set, 0.4 mm diameter wire, the measured inductance is 0.94 microHenry and the predicted value is 0.90 microHenry. For a  $\pm 1$  turn coil set with 1.1 mm diameter wire, the measured inductance is 0.79 microHenry. This shows that larger diameter wire will reduce the inductance. Anticipating a later result, it is seen that the decreased loss, due to the slightly decreased inductance, will be far overshadowed by the increased loss from the much larger conductance  $G$  of the copper core in the cable. Finally, the Rutherford cable coil was tested. It has the largest effective wire diameter, and exhibits the lowest inductance of 0.68  $\mu\text{H}$ , which is 28% lower than that of the single strand coil. This is of importance as it shows that larger wires marginally decrease inductance, but because of the close magnetic coupling, inductance is not decreased by a large factor.

### 3.2 Frequency Dependence of the AC Resistance $R_{ac}$

As pointed out in Section II, there are two important frequency regimes. In the frequency range where the hysteresis loss of the superconductor dominates, the resistance rises as frequency  $f$ . At higher frequency, or higher inductance values, the resistance rises as  $f^2$ . These are theoretical predictions. Figure 7 presents data which shows this theory is in reasonable agreement with the data.

### 3.3 Scaling Laws. Determination of Hysteresis Loss $R_{H0}$ & Shunt Conductance $G$ . Effect of Inductance $L$ and Cable Length $l_c$ on $R_{ac}$ .

Figure 8 summarizes representative data for a large number of experiments, in which the drive frequency was varied while the drive current was held constant at 30 Amps peak. The background magnetic field was 0 Tesla, and the temperature was held constant at 8° K. The frequency response of  $R_{ac}$  from 10 Hz to 10 kHz is presented.

It is obvious from the data at low frequencies, 10 to 100 Hz, that there is an uncertainty floor in  $R_{ac}$  around  $\pm 0.1 \mu\text{Ohm}$ , which arises from the baseline variation discussed earlier.

It is interesting to compare the  $\pm 1$  turn and  $\pm 4$  turn coils as to the scaling laws for cable length and inductance. Taking measured values for  $R_{ac}$  at 1000 Hz (which is well into the inductive-Ohmic loss regime), the AC resistance ratio  $R_{ac}(4 \text{ turns})/R_{ac}(1 \text{ turn})$  is  $\sim 15:1$ . From equation (5), the AC resistance is expected to scale as  $(\omega L)^2 G$ . The frequency  $\omega$  drops out of the ratio, and the measured inductance ratio  $[L(4 \text{ turns})/L(1 \text{ turn})]^2$  is  $\sim 75$ . The conductance  $G$  should *decrease* with increasing cable length, which gives a conductance ratio  $G(4 \text{ turns})/G(1 \text{ turn})$  of  $0.80 \text{ meter}/2.7 \text{ meter} \sim 0.3$ . Putting these together,  $[\frac{L_{4turn}}{L_{1turn}}]^2 \cdot [\frac{G_{4turn}}{G_{1turn}}] = 22 : 1$ , which is in reasonable agreement with  $\frac{R_{ac}(4turns)}{R_{ac}(1turn)} = 15 : 1$ , thus establishing the scaling laws for cable length and inductance.

It is found that the data of Figure 8 can be accurately and concisely summarized by fitting  $R_{ac}$  to an equation of form given in (7):

$$R_{ac} = R_{Series} + R_{H0} \cdot f + (\omega L)^2 \cdot G \quad (7)$$

It is found in practice that  $R_{Series}$  is negligible. Table 1 summarizes the measured inductance  $L$ , and the parameters  $R_{H0}$  and  $G$ , used in the fitting routine, which produce the best least mean squares fit to the data. The correlation coefficient  $r^2$  is presented to indicate the extremely good fit obtained. In parentheses ( ) are shown the same parameters on a per-length basis, which will be useful in calculating other coil geometries. A software package, TableCurve 2D<sup>(Registered)</sup> by Jandel Scientific, is used to perform the fitting.

| Coil & Wire Type                                   | $R_{H0}$<br>[Hysteresis Loss] | PF<br>[Power Factor] | G<br>[Shunt Conductance]   | L<br>[ Inductance] | $r^2$<br>[correlation coefficient] |
|--|-------------------------------|----------------------|----------------------------|--------------------|------------------------------------|
|  | [nanoOhm/Hz]                  |                      | [Siemens]                  | [microHenry]       |                                    |
| +/-1 turn coil,<br>old 0.4 mm wire.                | 5.56<br>(6.94 nΩ/Hz-m)        | 0.36                 | 0.116<br>(0.093 Siemens-m) | 0.94               | 0.97                               |
| +/-4 turn coil,<br>old 0.4 mm wire.                | 26.6<br>(9.90nΩ/Hz-m)         | 0.52                 | 0.038<br>(0.102 Siemens-m) | 8.16               | 0.99                               |
| +/-1 turn coil,<br>new 0.4 mm wire.                | 14.8<br>(18.5nΩ/Hz-m)         | 0.96                 | 0.305<br>(0.24 Siemens-m)  | 0.94               | 0.95                               |
| +/-1 turn coil,<br>1.1 mm wire.                    | 12.4<br>(15.5nΩ/Hz-m)         | 0.8                  | 0.722<br>(0.58 Siemens-m)  | 0.795              | 0.98                               |
| +/-1turn Ruther-<br>ford coil,<br>new 0.4 mm wire. | 6.98<br>(8.71nΩ/Hz-m)         | 0.45                 | 0.452<br>(0.36 Siemens-m)  | 0.678              | 0.99                               |

Table 1 - Results of Curve Fitting the AC Resistance Data by an Equation of Form:

$$R_{ac} = R_{H0} \cdot f + (\omega L)^2 \cdot G.$$

From Appendix B, equation. B-10, the measured hysteresis loss parameter  $R_{H0}$  is related to the internal inductance  $L_{int}$  as follows:

$$R_{H0} = 4 \cdot PF \cdot L_{int} \quad (8)$$

where

$$L_{int} = \left(\frac{\mu \cdot l_z}{8\pi}\right) \cdot \left(\frac{1}{1+\gamma}\right) \cdot \left\{1 + \frac{1}{3} \frac{\left(\frac{T_c}{T}\right)\gamma}{1+\gamma} \left(\frac{l}{l_c}\right)^2 + \dots\right\}$$

and

$$\gamma = \exp\left(\frac{T_c}{T}\right)$$

The Power Factor PF is defined as the fraction of the stored energy in the internal inductance, which is dissipated each cycle of the AC excitation. For  $T_c=18^0$  K,  $T=8^0$  K, and  $\mu = 400\pi$  (nH/m),  $L_{int}/l_z = 4.8$  nH/m. For the old 0.4 mm cable and the data of Table 1,  $R_{H0}/l_z = 6.94$  (nΩ/Hz-m), PF may be calculated as:

$$PF = 6.94/(4 \cdot 4.8) = 0.36 \quad (9)$$

which says about 1/3 of the energy stored in the internal inductance is dissipated each cycle for this particular superconductor.

### 3.4 Effect of Wire Diameter on AC Resistance

In Figure 8, the AC loss is compared for a cable 1.1 mm in diameter vs. a cable which is 0.4 mm in diameter. Because the 1.1 mm diameter cable has a very large diameter copper core, it has a much higher conductance  $G$  than the 0.4 mm cable which uses bronze as a jacket. It is apparent in Figure 8 that, counter-intuitively, the smaller wire has a lower loss! This points out that the cladding on the superconductor plays a large role in determining the AC resistance.

### 3.5 Dependence of AC Resistance on Temperature

Figure 9 compares  $R_{ac}$  vs. frequency as measured at equilibrium temperatures 8 and 12° K. This measurement was done on a  $\pm 4$  turn coil, which will exhibit loss dominated by the inductive-Ohmic effect. As is apparent in Figure 9, there is little increase in  $R_{ac}$  as the temperature increases to 12° K. Let us compare the measured result to theory.

From equation (B-10) of Appendix B, with  $I \ll I_c$ , the temperature dependence of  $R_{ac}$  is expected to be mainly in the hysteresis loss term  $R_{H0}$ :

$$R_{H0}(T) = 4 \cdot PF \cdot \left(\frac{\mu \cdot I_z}{8\pi}\right) \cdot \left(\frac{1}{1 + \exp\left(\frac{T_c}{T}\right)}\right) \quad (10)$$

$$\frac{R_{ac}(12^{\circ}K)}{R_{ac}(8^{\circ}K)} = \frac{(\omega L)^2 \cdot G + R_{H0}(12^{\circ}K) \cdot f}{(\omega L)^2 \cdot G + R_{H0}(8^{\circ}K) \cdot f} \quad (11)$$

From the data at 1000 Hz in Figure 9, the measured values  $R_{ac}(8^{\circ} K) = 124 \mu\Omega$ ,  $R_{ac}(12^{\circ} K) = 143 \mu\Omega$ . By calculation from the data in Table 3.1 for the  $\pm 4$  turn coil:

$$R_{ac}(8^{\circ} K) = 99.9 \mu\Omega + 26.6 \mu\Omega = 126 \mu\Omega.$$

$$R_{ac}(12^{\circ} K) = 99.9 \mu\Omega + 50.8 \mu\Omega = 150.7 \mu\Omega, +20\% \text{ change.}$$

So, the theoretical model of Appendix B fits the temperature dependence fairly well. It shows that only at the lower frequencies will there be any large temperature induced changes in the AC resistance of a superconductor.

### 3.6 Dependence of AC Resistance on DC Magnetic Flux Density $B_0$

Increasing the DC magnetic flux density  $B_0$  applied to the  $\pm 1$  turn coil produced a slight increase in the measured  $R_{ac}$ . Figure 10 illustrates the data for a  $\pm 1$  turn coil, operated with a bias current of 64 Amps and a peak AC current of 60 Amps. The external magnet could produce a z-directed DC magnetic flux density at any value from 0 to 1.5 Tesla, depending on the current applied. Measurements of  $R_{ac}$  vs frequency were made extensively at  $B_0 = 0$  and 0.5 Tesla. Points were also taken at  $B_0 = 1$  and 1.5 Tesla, fixed frequency of 400 Hz.

The data can be fitted by a quadratic dependence of  $R_{ac}$  on DC magnetic flux density  $B_0$  as:

$$R_{ac} = R_{H0} \cdot [1 + 0.93 \cdot B_0^2] \cdot f + (\omega L)^2 \cdot G \quad (12)$$

where:  $R_{H0} = 5.60 \text{ n}\Omega/\text{Hz}$ ,  $f$  in Hertz,  $L = 0.94 \mu\text{H}$ ,  $G = 0.11 \text{ Siemens}$ ,  $B_0$  is in Tesla,  $\omega$  is in radian/sec. The dependence of  $R_{ac}$  on  $B_0$  is seen to be mainly at the low frequency end, where hysteresis loss dominates.

### 3.7 Dependence of AC Resistance on Current $I_p$

Figure 11 illustrates the dependence of  $R_{ac}$  on AC peak current amplitude  $I_p$ . It is observed that the measured loss resistance  $R_{ac}$  increases with increasing current amplitude  $I_p$ , as expected from the theory of Appendix B.

To quantify the current dependence,  $R_{ac}$  is measured at various drive current values,  $I_p$ , up to 50 Amps. At each fixed current drive level, the hysteresis coefficient  $R_{H0}$  is determined. From the wire manufacturer's data sheet, it is determined that the critical current for the new 0.4 mm superconducting cable is of the order of 100 to 200 Amps. Using  $I_c = 100$  Amps, the set of measured values  $R_{H0}(I_p)$  was fitted by a functional form of  $R_{H0}(I_p)$  given in equation (B-10). A reasonable fit to the measured data is achieved with the fourth order equation shown:

$$R_{H0} = R_{H0}^{(small\_signal)} \left\{ 1 + 0.68 \left(\frac{I_p}{I_c}\right)^2 + 20.5 \left(\frac{I_p}{I_c}\right)^4 + \dots \right\} \quad (12)$$

where

$$R_{ac} = R_{H0} \cdot f + (\omega L)^2 \cdot G \quad (13)$$

The result shows that the non-linear increase of  $R_{ac}$  with current  $I_p$  can be mainly ascribed to the hysteretic loss in the internal inductance of the superconductor. Since care is exercised to maintain the temperature constant, the effect is clearly due to the B vs H hysteresis nature of the superconductor and not to an uncontrolled thermal effect.

### 3.8 Conclusions drawn from the Experimental Data

Superconducting cable can be well modeled by the shunt/series circuit of Figure 4 and equation (5). Using an equivalent series resistance  $R_{ac}$  is a good model of the power loss.  $R_{ac}$  may be divided according to two major loss mechanisms. **Hysteresis loss** is seen predominantly at frequencies in the ten to hundreds of Hertz region, and has a linear frequency dependence,  $f$ . It arises from flux trapping in the superconductor. **Inductive-Ohmic loss** is the major determinant of loss, is due to the normal metal jacketing of the superconductor, and has a quadratic frequency dependence,  $f^2$ . An applied DC magnetic flux intensity  $B_0$  of up to 1.5 Tesla, has a minor, second order affect on the AC loss characteristics of a superconducting cable. Therefore, superconducting gradient coils will be useful in practical MRI polarizing fields of 1.5 Tesla or greater.

As long as the temperature at which the  $Nb_3Sn$  superconductor is operated is less than  $12^0K$ , there will be only a minor second order increase in AC loss.

Of greatest importance is the result that the AC resistance increases steeply with drive current amplitude, approximately as  $I_p^4$ , above  $\sim 30$  Amps peak current in the cable measured in this work. This means that to achieve high total currents, of the order  $\sim 1000$  Amps, paralleling of many cables will be necessary. The major concern becomes that of assuring an even sharing of the current among the conductors, to avoid quenches from overloaded individual superconductors. More research is needed on this subject.

The foregoing data may be combined into one equation summarizing the AC resistance of superconducting cable formed into a structure with known inductance  $L$  and cable length  $l_z$ , operated with a sine wave current drive of amplitude  $f$ , amplitude  $I_p$ :

$$R_{ac} = \left\{ \left[ R_{H0}^{(small\_signal)} \cdot f \right] \cdot \left[ 1 + 0.68 \left( \frac{l_z}{l_c} \right)^2 + 20.5 \cdot \left( \frac{l_z}{l_c} \right)^4 \right] \cdot \left[ 1 + 0.93 \cdot B_0^2 \right] \right\} + \{ (2\pi \cdot f \cdot L)^2 \cdot G \} \quad (14)$$

with 
$$R_{H0}^{(small\_signal)} = 4 \cdot PF \cdot L_{int}^{(small\_signal)}$$

where PF is the power factor, of the order of 0.1 to 0.5, and the internal inductance  $L_{int}^{(small\_signal)}$  is:

$$L_{int}^{(small\_signal)} = \left( \frac{\mu \cdot l_z}{8\pi} \right) \cdot \frac{1}{1 + \exp\left(\frac{T_c}{T}\right)}$$

$\mu$  = free space permeability,  $T_c$  = the transition temperature, and  $T$  = the superconductor temperature.

## 4 Discussion

Measuring the AC loss of a superconductor is difficult due to the extremely small dissipation expected and observed. To overcome the problems of ultrahigh accuracy in measuring a phase angle near  $90^0$  as in an impedance based measurement, a calorimetric method is presented and utilized. Since a direct measurement of heat is made by the calorimeter, along with a measurement of the transport current, the electrical resistance can be directly inferred. The accuracy is limited mainly by the thermal stability of the apparatus, which is of the order of 1%. Because the measurement is made isothermally, it is possible to apply large currents, apply an external magnetic field, or to choose a precise temperature of operation without invalidating the results. In this circumstance, one can be certain that the AC resistance measured is due to the effect of the particular input parameter, not due to an uncontrolled temperature change.

The price paid for a direct measurement based on thermal techniques, is that the measurements can be made only as fast as the thermal time constant of the apparatus allows. This is of the order of 1 to 3 minutes. In addition, the feedback controller can be set to have a long integration time to smooth out the random variations, a process which improves the measurement accuracy but slows the data acquisition. In a typical measurement sequence, twenty one discrete frequencies from 10 Hz to 10 kHz would be chosen. With no AC current applied, a baseline value for  $P_0$  would be established, typically in 5 to 10 minutes. Then a frequency, e.g. 10 Hz, and an AC current amplitude, e.g. 20 Amps, would be selected and applied to the coil set. With no transfer gas in the apparatus, thermal equilibrium would be regained in 10 to 15 minutes. With transfer gas, the equilibrium only took about 2 to 4 minutes to achieve because of the higher cooling rate. Obtaining one baseline reference point (no AC current applied) and a full set of AC resistance values at the one current amplitude and twenty one selected frequencies, could take 1 to 2 hours. Multiplying this by some number of current amplitudes, e.g. 5, several different background fields  $B_0$ , e.g. 4, and two or three temperatures, the time to evaluate one sample completely could take 50 to 100 hours. An automated system helps solve this problem, as measurements can be made overnight in an unattended mode.

To summarize, the calorimetric measurement approach provides an accurate, absolute measurement of the AC resistance of a superconductor. It is slow because of the need to attain thermal equilibrium. The most critical item is the temperature controller, which must have low noise and high baseline stability. Further improvements are needed in this area.

A simplified theory of AC losses in superconductors is presented. It provides a framework in which the results of the measurements may be interpreted, and it provides a basis for some extrapolation of results to other conditions. It is simplified in that the precise mechanisms for flux pinning in "hard" superconductors are not included. It seems to predict the hysteretic losses in the superconductor reasonably well, within the limit of an empirically determined power factor, PF, which is in the range 0.1 to 1. Further refinement of the theory is expected to relate the number, size, and dislocation density of the filaments in the superconductor to PF.

The main features exhibited both by the measured AC resistance and the values predicted by the theory are that: 1)  $R_{ac}$  increases with frequency  $f$  in the low audio range and as  $f^2$  in the high audio range of frequencies, 2) there is a strong dependence of  $R_{ac}$  on AC current amplitude  $I_p$ , and 3) that either the temperature or the external DC magnetic field intensity has a rather small effect on the AC resistance.

Finally, the results for three commercially available,  $Nb_3Sn$  filamentary superconducting cables are presented. It is found that the lowest loss cables have the least amount of high conductivity, normal metal incorporated. The cable can be characterized by two parameters,  $R_{H0}$  due to hysteresis loss in the superconductor, and a shunt conductance  $G$ , due to the normal metal incorporated in the cable. Values for these parameters, normalized to a per unit length basis, are presented.

## 5 Acknowledgments

This project was taken on jointly by H-P Labs and Cryogenic Ltd.. T. A. Shoup of H-P, was quite instrumental in suggesting effective goals, and in structuring the project between H-P and Cryogenic Ltd.. H. E. Melton, at H-P Laboratories, contributed support and helped with critical reviews of the project as it went along. M. Owczarkowski of Cryogenic Ltd., provided much help with the high current drivers and the measurement electronics. The staff at Cryogenic Ltd., and at H-P Laboratories, deserve a special note of thanks for their support.

## Appendix A - Details of READ Gradient for the Echo Planar Sequence

As an example of harmonic content in a trapezoidal driving waveform for an EPI sequence, assume  $G_{read}$  is 17 mT/m, and the period is  $2T_{Line} = 1563 \mu s$ . Assume that the efficiency of the gradient coil is given, so that a current of amplitude  $I_0$  will produce a flat top gradient amplitude of 17 mT/m. Figure A.1 illustrates the repetitive, trapezoidal current waveform  $I(t)$ , which can be represented by a Fourier series in terms of fundamental frequency  $f_1$  and harmonics  $f_n = n \cdot f_1$ :

$$I(t) = \sum_n I_n \cdot \sin(2\pi \cdot n \cdot f_1 \cdot t) \quad (A.1)$$

In this example, the fundamental frequency is  $f_1 = 640 \text{ Hz}$ .

Anticipating a calculation of power, which is proportional to  $I_n^2$ , Table A.1 shows the relative harmonic content of  $(I_n^2)$ . Note that the amplitude of  $I_n^2$  drops rapidly to about 5% of that in the fundamental  $I_1$ , then declines very slowly for harmonic numbers  $n > 5$ . The power dissipated depends on the AC resistance  $R_n$  presented to the harmonic current at each frequency  $f_n$ :

$$P = \frac{1}{2} \sum_n (I_n)^2 \cdot R \quad (A.2)$$

where  $P$  is the average power dissipated,  $I_n$  is the peak current carried by the  $n^{\text{th}}$  harmonic, and  $R_n$  is the resistance presented by the coil at the  $n^{\text{th}}$  harmonic,  $f_n$ .

| n  | $f_n$ (Hz) | $(I_n/I_0)^2$ |
|----|------------|---------------|
| 1  | 640        | 1.599         |
| 3  | 1920       | 0.159         |
| 5  | 3200       | 0.046         |
| 7  | 4480       | 0.016         |
| 9  | 5760       | 0.006         |
| 11 | 7040       | 0.002         |
| 13 | 8320       | 0.0004        |
| 15 | 9600       | 0             |
| 17 | 10880      | 0             |
| 19 | 12160      | 0.0001        |

Table A.1 - Harmonic Content of a Trapezoidal Wave of Rise Time and Repetition Frequency Described in the Text.

If one assumes that the circuit presents a uniform resistance  $R_n = R_0$  vs frequency (a good approximation for a copper conductor), the power dissipated by the trapezoidal waveform is  $0.92 \cdot I_0^2 R_0$ . For a flat topped, square wave driving current, the dissipation would be  $I_0^2 R_0$ .

For a superconducting coil, a detailed calculation of equation (A.2) for a bandwidth limited driving waveform, yields the power dissipation as:

$$P_{diss} = \{ 1.20 \cdot (R_{H0} \cdot f_1) + 2.89 \cdot (2\pi \cdot L \cdot f_1)^2 \cdot G \} \cdot I_0^2 \quad (A.3)$$

which can be two to three orders of magnitude smaller than that for a comparable copper coil set.

**Appendix B - Calculation of the Internal Stored  
Energy & Hysteresis Loss in a Superconducting Cable**

A transport current  $I$  flows in a superconducting cable of diameter  $d$ . The transport current creates a magnetic intensity  $H$  within the cable. In turn,  $H$  induces a magnetic flux density  $B$ , and energy is stored in the field. To model the superconductor by an electric circuit, the internal stored energy is needed. To calculate the stored energy, a relation between  $B$  and  $H$  is needed. As pointed out by Norris<sup>12</sup>, type II superconductors are difficult to model because of the large number of pinning sites present, and the uncertainty as to the details of flux penetration into the bulk of the superconductor. A simplified relation will be developed.

Superconductivity is thought to arise from the flow of Cooper pair electrons, which can be considered as a quasi-particle "gas" that obeys modified Fermi-Dirac statistics, see Kittel<sup>8</sup> and Rose<sup>9</sup>. For the simplified theory of a superconducting cable presented here, the following constitutive relation between  $B$  and  $H$  in the superconductor is used:

$$B(H) = \mu \cdot \frac{H}{\left\{1 + \exp\left[\left[1 - \left(\frac{H}{H_c}\right)^2\right] \cdot \left(\frac{T_c}{T}\right)\right]\right\}} \quad (\text{B-1})$$

where  $\mu$  is the permeability of free space,  $T$  is the operating temperature in degrees K,  $T_c$  is the critical temperature in degrees K, and  $H_c$  is the critical field. Above either critical point, the superconductor reverts to a normal metal state. Figure B-1 illustrates this relation for a hypothetical superconductor with  $T_c = 18^\circ\text{K}$ , and operating temperatures of 1, 8, or  $18^\circ\text{K}$ .

At any given point within the superconductor, the energy stored per unit volume,  $w(H_m, T)$ , is the work done in bringing the magnetic field intensity from 0 to  $H_m$ :

$$w(H_m, T) = \int_0^{H_m} B(H, T) dH \quad (\text{B-2})$$

which can be integrated by substituting  $B(H)$ , as given in equation (B-1). Using Mathcad 5.0 PLUS<sup>(registered)</sup> and the MAPLE V R3<sup>(registered)</sup> symbolic processor, equation (B-2) is carried out analytically. The result is expanded about  $H=0$  in a power series in order to determine the linear and non-linear portions of the model:

$$w(H_m, T) = \frac{1}{2} \left[ \frac{\mu}{1+\gamma} \right] \cdot H_m^2 \cdot \left\{ 1 + \frac{1}{2} \left( \frac{T_c}{T} \right) \cdot \left[ \frac{\gamma}{1+\gamma} \right] \cdot \left( \frac{H_m}{H_c} \right)^2 + \dots \right\} \quad (\text{B-3})$$

where:  $\gamma = \exp\left(\frac{T_c}{T}\right)$ .

To calculate the  $H$  field throughout the cable, assume that a transport current  $I$  is distributed with uniform current density  $J(r) = J_0$  across the cross section of the cable. The cable has outer radius  $r_0$ , diameter  $d = 2r_0$ , and a cross sectional area of  $A = \pi r_0^2$ . The  $H_m$  field is then given by:

$$H_m(r) = \left\{ \frac{I}{A} \right\} \cdot \left( \frac{r}{2} \right) \quad (\text{B-4})$$

The critical field  $H_c$  is related to the critical current  $I_c$  by:

$$H_c = \frac{I_c}{2\pi r_0} \quad (\text{B-5})$$

These relations are substituted into the energy per volume,  $w(H_m, T)$ , which is integrated over the volume of the cable to obtain the total stored energy  $E(I, T)$ . Integrating in cylindrical coordinates with volume element  $2\pi r \cdot dr \cdot dz$ , the energy is:

$$E(I, T) = \frac{1}{16} \left( \frac{\mu \cdot l_z}{\pi \cdot (1+\gamma)} \right) \cdot (I^2) \cdot \left\{ 1 + \frac{1}{3} \frac{\left( \frac{T_c}{T} \right) \gamma}{1+\gamma} \cdot \left( \frac{I}{I_c} \right)^2 + \dots \right\} \quad (\text{B-6})$$

The cable is assumed to be of length  $l_z$

Viewing the cable as a circuit described by the internal inductance  $L_{int}$  and a current  $I$  flowing into the terminals, the energy is given by  $\frac{1}{2} L_{int} I^2$ . The internal inductance is found as:

$$L_{int} = \frac{2E(I, T)}{I^2} = \left( \frac{\mu \cdot l_z}{8\pi} \right) \cdot \left( \frac{1}{1+\gamma} \right) \cdot \left\{ 1 + \frac{1}{3} \frac{\left( \frac{T_c}{T} \right) \gamma}{1+\gamma} \left( \frac{I}{I_c} \right)^2 + \dots \right\} \quad (\text{B-7})$$

Figure B-2 (a) illustrates  $L_{int}$  vs transport current  $I$ , while Figure B-2 (b) illustrates  $L_{int}$  vs temperature. In both cases, the cable length is taken to be  $l_z = 0.8$  meters. Both plots show the classic internal inductance,  $\frac{\mu \cdot l_z}{8\pi}$ , as the limiting value. When the temperature  $T$  is near absolute zero ( $\gamma \rightarrow \infty$ ), and the transport current  $I$  is small compared to the critical current, the superconductor almost completely excludes any flux from its interior. In turn, the internal inductance approaches zero as shown by (B-7). Conversely, as the temperature approaches the critical temperature  $T_c$ , the superconductor only partially excludes flux, and the internal inductance increases toward the classic limiting value,  $\frac{\mu \cdot l_z}{8\pi}$ . Likewise, as the transport current  $I$  increases toward  $I_c$ , the flux is not excluded as completely and the internal inductance rises.

In general, the energy stored in the internal inductance of the superconducting cable is non-dissipative, that is, all the energy stored in bringing the field to the maximum value  $H_m$  can be recovered when the field decreases back to zero. However, due to magnetic pinning sites and crystal imperfections discussed earlier, there is some energy lost as the field is changed from high to low, or low to high. The effect can be described by a hysteresis loop in the  $B - H$  constitutive relation. If a periodic driving  $H$  field is applied to the superconductor, in one complete cycle the material will be carried once around the  $B-H$  hysteresis loop. This will result in an amount of energy, proportional to the area enclosed by the hysteresis loop, to be dissipated. If no magnetic imperfections were present, the area under the loop would drop to zero and no energy would be dissipated.

At this point, the assumption is made that the dissipated energy is proportional to the change in stored energy. This assumption allows one to define a power factor,  $PF$ , which empirically characterizes the quality of the material.  $PF$  is 0 for a superconductor exhibiting no hysteresis, and can range up to 1 for a superconductor which dissipates all the stored energy in one transit around the hysteresis loop. The energy lost per cycle may be written as:

$$E_{diss} = 4 \cdot PF \cdot E(I, T) = 4 \cdot PF \cdot \left( \frac{1}{2} \cdot L_{int} \cdot I^2 \right) \quad (\text{B-8})$$

The factor 4 arises because the stored energy is increased to a maximum twice, and decreased to zero twice during one cycle around the hysteresis loop. During each of these four changes, the pinning sites resist the change, and an increment of energy  $PF \cdot E(I, T)$  is lost.

If the hysteresis loop is traversed at a frequency  $f$  cycles per second by application of a periodic (sinusoidal) driving function  $H$ , the power dissipated is simply:

$$P_{diss} = 4 \cdot PF \cdot \left( \frac{1}{2} \cdot L_{int} \cdot I^2 \right) \cdot f \quad (\text{B-9})$$

It is natural to model this electrically as a resistance  $R_H$  connected in series with the internal inductance  $L_{int}$ , so the power dissipated can be expressed as:

$$P_{diss} = \frac{1}{2} \cdot I^2 \cdot R_H \quad (\text{B-10})$$

where:

$$R_H = \left( \frac{2PF}{\pi} \right) \cdot L_{int} \cdot \omega$$

$$R_{H0} = 4 \cdot PF \cdot L_{int}$$

$$L_{int} = \frac{2E(I,T)}{f^2} = \left(\frac{\mu \cdot l_z}{8\pi}\right) \cdot \left(\frac{1}{1+\gamma}\right) \cdot \left\{1 + \frac{1}{3} \frac{\left(\frac{T_c}{T}\right)^\gamma}{1+\gamma} \left(\frac{I}{I_c}\right)^2 + \dots\right\}$$

The main result of Appendix B is that the hysteresis component of dissipation in a superconductor can be modeled as a series resistance. The important relations are: 1) the loss increases linearly with frequency  $f$ , 2) the loss increases linearly with the cable length  $l_z$  but depends only slightly on the cross-sectional area, 3) the loss increases modestly with temperature in the range  $T > 0.5 T_c$ , and 4) the resistance is non-linear in the drive current. The non-linear effect brings in the critical current as a normalizing term, and shows that conductors with a high critical current will have less non-linear loss.

The external inductance must also be included. In general, the superconducting cable will be wound into a coil, a loop, or other geometric form, which will create an external magnetic field. The energy stored in the external field is characterized by the coil current  $I$ , and the external inductance  $L_{ext}$  which may be calculated from the geometrical current distribution<sup>21</sup>. The external inductance is generally many times greater than the internal inductance, and dominates the measured inductive-Ohmic loss of the coil(s) under test.

**Appendix C -  
Maxwell Pair Gradient Coil as an  
Experimental Vehicle to Evaluate  
Superconducting Cable.**

**C1 Maxwell Pair Gradient Coil as a Circuit to Determine AC Resistance**

To measure superconducting cable electrical loss, an experimental model was needed. A Maxwell pair was chosen because of its utility in MRI to produce a z-gradient. Further, the Maxwell pair has an analytical solution for the external inductance  $L_{ext}$  and the gradient strength  $G_z$ , is easily fabricated from superconducting cable by contra-winding two coils of radius  $a$  spaced  $\sqrt{3} \cdot a$  apart along the z-axis, and is readily scaled in size. For reasonable current and cost levels, a radius  $a = 50mm$  was chosen.

To test the effect of a z-directed DC magnetic field on the AC resistance, a superconducting magnet was included in the apparatus. It produces fields up to 1.5 Tesla, with a sensitivity of 38.5 mT/Amp.

**C2 Parameters of a Maxwell Coil Set**

The important circuit parameters will be calculated. In Figure 3 is a schematic drawing of a Maxwell pair. Figure 4 is an equivalent electrical circuit which will be made quantitative.

The *external inductance*  $L_{ext}$  is composed of the self inductance of each loop, the mutual inductance between the loops, and the inductance of the pair of wires interconnecting the two coils. The latter inductance is small because the wires are pushed close together to minimize the area, but non-zero because there is an unavoidable minimum spacing. The self inductance of a loop and the mutual inductance between the two contra-wound loops is given analytically<sup>22</sup>. The inductance of the connecting wires is derived approximately in this work. The total external inductance of the Maxwell pair as seen at the terminals is:

$$L_{ext} = \left(\frac{\pi}{2}\right) \cdot \mu \cdot a \cdot N_l^2 \left\{ \ln\left[\frac{16 \cdot a}{d}\right] - 2 - \frac{\pi}{16} \right\} + \left(\frac{\pi}{2}\right) \cdot 2 \cdot \sqrt{3} \cdot \mu \cdot a \cdot N_c^2 \cdot \left\{ \ln\left[\left(\frac{S}{a}\right)^2 - 1 \right] \right\} \quad (C-1)$$

loop self and mutual + interconnect pair inductance..

Here,  $N_l$  is the number of turns in each coil,  $S$  is the centerline-to-centerline spacing of the interconnecting wires, and  $N_c$  is the number of interconnecting pairs. Note that this result has been modified by about 20% from that of Ramo and Whinnery<sup>21</sup> through the factor  $\left(\frac{\pi}{2}\right)$  {two coils times  $\left(\frac{\pi}{4}\right)$  per coil}, which is found to better fit the calculated inductance to the measured values.

As an example, for the  $\pm 1$  turn coil set ( $N_l=1$ ) used in this study - with loop radius  $a = 50$  mm, superconducting cable diameter  $d = 0.4$  mm, single interconnect pair  $N_c = 1$ , spacing  $S = 2d$  - equation (C-1) predicts:

$$L_{ext} = 0.53 \mu\text{H} \quad + \quad 0.37 \mu\text{H} \quad = \quad 0.90 \mu\text{H}.$$

loops + interconnects

The *internal inductance*  $L_{int}$  arises from energy storage within the interior of the superconducting cable. In a normal metal with uniform current density throughout the cross-section of a wire, the internal inductance is given by<sup>21</sup> as:

$$L_{int}^{(N)} = \left(\frac{\mu \cdot l_z}{8\pi}\right) \quad (C-2A)$$

and for a superconductor as:

$$L_{int}^{(S)} = \left(\frac{\mu \cdot l_z}{8\pi}\right) \cdot \left(\frac{1}{1+\gamma}\right) \cdot \left\{ 1 + \frac{1}{3} \frac{\left(\frac{T_c}{T}\right) \gamma}{1+\gamma} \left(\frac{l}{l_c}\right)^2 + \dots \right\} \quad (C-2B)$$

where  $\mu$  is the permeability of free space,  $T$  is the operating temperature,  $T_c$  is the transition temperature. The total length of the conductor is  $l_z$ , which can be expressed as:

$$l_z = \{2\pi \cdot a \cdot N_l + \sqrt{3} \cdot a \cdot N_c\} \cdot 2 \quad (C-3)$$

( 1 coil + 1 interconnect wire) x 2.

In the idealized superconductor, the internal inductance is zero at  $T = 0^0$  K, rising toward the value  $(\mu_l)/(8\pi)$  as the temperature increases to  $T_c$ . Appendix B presents the temperature, field, and current dependence of  $L_{int}$ . For the example coil,  $L_{int} < 0.004 \mu\text{H}$ , so it has little effect on the total inductance seen at the terminals.

The *hysteretic resistance*  $R_H$  of the superconductor depends directly on the internal inductance  $L_{int}$  as shown in Appendix B.  $R_H$  is temperature, field, and current sensitive. It increases linearly with length of conductor, and with frequency. It depends only slightly on the cross-sectional area of the superconducting cable, but does decrease as the number of superconducting filaments increases. For the example coil with radius  $a = 50$  mm, the expected resistance is in the 1 micro-Ohm range at 100 Hz.

The *shunt conductance*  $G$  is due to the normal metal jacket. In the case of the  $\text{Nb}_3\text{Sn}$  discussed in this paper, the normal metal is the bronze (copper/tin) core in which the superconducting filaments are encased. The conductance  $G$  depends on the normal metal conductivity  $\sigma$  at cryogenic temperatures, on the effective cross-sectional area of the conductor, and the conductor length  $l_z$ . If the normal metal occupies a fraction  $X$  of the cross-sectional area of the superconducting cable, the conductance  $G$  is given by:

$$G = \sigma \cdot (X) \cdot (\pi \frac{d^2}{4}) / (l_z) \quad (C-4).$$

In general, having as small a conductance,  $G$ , as possible is desired. The conductance  $G$  decreases as the conductivity  $\sigma$  decreases, as the conductor becomes longer, i.e. as more turns are added, as the fraction of area  $X$  occupied by normal metal decreases, i.e. as the metal jacket is removed, and as the diameter  $d$  is decreased. Decreasing the cable diameter  $d$  has the effect of decreasing the number of fixed diameter superconducting filaments which can be placed in the cable, and causes a concomitant increase in the hysteretic loss  $R_H$ . Decreasing  $d$  also decreases the critical current  $I_c$  of the superconductor, which reduces the current carrying ability of the cable and increases the non-linear loss term in  $R_H$ . (See Appendix B). There is clearly a compromise value of diameter  $d$  which leads to minimum loss.

#### C4 Analysis of Circuit Model

In the experimental determination of AC electrical loss in superconductors, the power dissipated in the superconductor is measured. Since the superconductor is expected to have very low impedance, in the milliOhm region, exciting it with a current source is the appropriate method. For sinusoidal excitation with a current of form:

$$I_p(t) = I_p \cdot \sin(\omega \cdot t) \quad (C-5)$$

the power dissipated is:

$$P_{diss} = \frac{1}{2} \cdot \text{re}\{V_L \cdot I_p^*\} + |I_p|^2 \cdot R_{Series} \quad (C-6)$$

The complex impedance  $Z'$  is defined as:

$$Z' = \frac{(j\omega L + R_H) \cdot \frac{1}{G}}{j\omega L + R_H + \frac{1}{G}} \quad (C-7)$$

and

$$V_L = Z' \cdot I_p \quad (C-8)$$

so

$$P_{diss} = \frac{1}{2} \cdot \text{re}\{Z' + R_{Series}\} \cdot |I_p|^2 \quad (C-9)$$

and

$$R_{ac} = \frac{2 \cdot P_{diss}}{|I_p|^2} = \text{re}\{Z' + R_{Series}\} \quad (C-10)$$

Equation (C-10) is the key to interpreting the measured data,  $P_{diss}$  and  $I_p$ . Putting the expression in (C-7) on a common denominator, substituting it into (C-9), and extracting the real part, the AC resistance  $R_{ac}$  is expressed as:

$$R_{ac} = \frac{R_H \cdot [1 + G \cdot R_H] + (\omega L)^2 \cdot G}{[1 + G \cdot R_H]^2 + [\omega L \cdot G]^2} + R_{Series} \quad (C-11)$$

It should be noted that for the 100 mm diameter gradient coil set,  $G \sim 0.1 - 1$  Siemens,  $\omega L \sim 0.1$  Ohm maximum, and  $R_H \sim 10$  micro-Ohm, so many of the above terms are negligible.  $R_{ac}$  then reduces to:

$$R_{ac} \approx R_{Series} + R_H + (\omega L)^2 \cdot G \quad (C-12)$$

where:

$$L = L_{ext} + L_{int} \quad .$$

**Appendix D -**  
**Calorimetric Measurement of AC Loss -**  
**Experimental Apparatus and Operation.**

Various types of calorimeter have been described in the literature. Most of these simply measure the rate of helium gas evolution<sup>23</sup>, and relate that to the power dissipated in the cryostat. Limited sensitivity and uncontrolled temperature excursions of the sample are major drawbacks to these methods. In this work, a feedback calorimeter is introduced to overcome such problems.

The calorimetric measurement device is described in more detail. It is built on a fiberglass support tube. A mono-layer of insulated, 0.2 mm diameter copper wire, is glued longitudinally along the tube to provide good thermal conduction between the Maxwell pair, the heater coils, and the thermal link to thermal ground. A longitudinal configuration of wires is chosen to suppress eddy currents, which could provide an extraneous source of electrical dissipation. Thermometers are provided to monitor the temperature. In Figure D-1, the fiberglass former, one of the thermal sensors, and the supporting top plate are shown.

A non-inductive heater coil is epoxied in place at each end of the fiberglass tube. Each heater consists of 8 turns of resistance wire, and presents about 30 Ohms resistance to the Conductus LTC-10 driver. Two Cernox<sup>(Registered)</sup> ruthenium oxide thin film resistance temperature sensors are installed, one near each of the two heaters, as the means to monitor the system temperature. The device resistance is monitored by a four terminal measurement system, and the resistance is converted to degrees Kelvin through a software calibration routine in the Conductus LTC-10 temperature controller.

The Maxwell pair gradient coils are wound on a metal mandrel, then reacted in a furnace, to form the Nb<sub>3</sub>Sn alloy desired. The coils are somewhat brittle, but flexible enough to be handled.

The gradient coils are carefully slid off the mandrel onto the fiberglass former tube, and epoxied in place. Each heater coil is placed about 5 cm from its adjacent coil in the Maxwell pair. In this configuration, the coils are reasonably well coupled thermally. The entire assembly is mounted on a top plate which has electrical feed-throughs to the outside, and which forms part of the vacuum isolation chamber. The vacuum enclosure is completed by a stainless steel can which is bolted to the top plate. An indium metal gasket is used to seal the joint between the can and the top plate. Indium is used because it remains malleable enough at cryogenic temperatures to provide a good seal.

With the gradient coils and heater coils in place, electrical cross-coupling was checked. The mutual inductance between the heater and gradient coil was measured with an HP 4284A LCR meter, used in a four terminal configuration. For the ±4 turn Maxwell pair, the gradient coil self inductance was measured to be  $L_G = 3.8 \mu\text{H}$  per coil, the heater coil self inductance was measured to be  $L_H = 4.2 \mu\text{H}$  per coil, and the mutual inductance between the two measured to be  $M = 0.01 \mu\text{H}$ . With a heater resistance  $R_H = 30 \text{ Ohms}$ , and a maximum measurement frequency (worst case) of 10 kHz, electrical cross-coupling would contribute an additional  $[(\omega M)^2/R_H] \sim 13 \text{ nanoOhms}$  to the measured series resistance, a negligible amount for this system.

To make the power dissipation measurement calorimetrically, a thermal path is established by a thermal resistance  $R_T$  to the thermal ground, i.e., the surrounding container held at 4.2° K by the liquid helium bath. When a certain amount of power  $P_{diss}$  is dissipated inside the container, the temperature  $T$  will rise according to the following equation:

$$(T - T_0) = R_T \cdot P_{diss} \quad (\text{D-1})$$

where  
and

$$T_0 = 4.2^\circ \text{ K}$$
$$R_T \sim 0.4^\circ \text{ K}/(\text{milliWatt}).$$

In this apparatus, the thermal resistance is provided by a copper wire which links the fiberglass former to the top plate. About 10 to 12 milliWatts of heater power are needed to maintain the temperature at 8° K. To achieve a stable baseline, helium gas must be excluded to prevent convective heat transfer. Thus, the need for a vacuum enclosure. As it turned out, for measurements at frequencies above a few hundred Hertz, power dissipation on the order of 200 mW was experienced. To increase the dynamic range of the measurement, a very small (~1 mm<sup>3</sup>) amount of helium transfer gas was admitted inside of the vacuum vessel. This provided an additional convective cooling path from the coils to the can walls. The thermal resistance decreased by an order of magnitude, thus allowing measurements at higher frequencies/higher powers to be made.

At the low frequency end of the range (10 to 100 Hz), the power dissipated in the superconductor was so low that thermal drift of the system became an issue. In the state where no helium gas was admitted to the inside of the container, the power to maintain a constant temperature was stable to about +/- 0.1 mW. This required continuous pumping on the container to remove adsorbed residual helium gas which outgassed from the coils and former. It also set the most important limit on the measurement accuracy. With He gas present, the stability was decreased to about +/-0.5 mW, out of ~ 200 mW total power required to maintain the 8° K temperature.

In order to test the effect of DC fields up to 1.5 Tesla, a superconducting solenoid magnet was placed coaxially around the container housing the gradient coils. The DC field is directed in the z-direction, relative to the gradient coils, so the gradient coils see exactly the magnetic environment of an MRI scanner. The DC field is excited by a separate set of leads into the cryostat, and a special purpose power supply is used to ramp the field up at a controlled rate. A persistent switch is provided so that the magnet can be held at a constant field without continuous excitation. The transfer parameter for the DC coil is 38.5 mTesla/Amp of current. Figure D-2 illustrates the entire unit assembled, with the DC solenoid magnet over the chamber holding the gradient coil apparatus.

To operate the apparatus, the unit is lowered into the cryostat, and pre-cooled with liquid nitrogen. When the system temperature reaches 77° K, the liquid nitrogen is forced out by pressurizing the system with helium gas. This purges the nitrogen and leaves the system ready for helium transfer. A transfer siphon is inserted into the cryostat, and helium is transferred until the can is completely covered. A level detector monitors the height of the liquid helium. It is found that the can must be covered completely, in order to avoid a source of baseline drift.

## List of Figure Captions

Figure 1 - Illustrating the Penetration of Flux into a Superconductor as Controlled by Fluxoids. (a) Small Drive Field, (b) Drive Field Increases, (c) Drive Field at Maximum.

Figure 2 - Illustrating the Magnetic Field Generated by a System of Twisted Conductors.

Figure 3 - Schematic Diagram of a Maxwell Pair Gradient Coil Set. Coils are Series Connected, with Current Flow in Opposite Sense in Top and Bottom Coils. Coil Radius is  $a$ , Coil Spacing is  $\sqrt{3} a$ . In the Region Between the Two Coils, a Linear Variation in the z-directed Magnetic Field is Produced.

Figure 4 - Circuit Model for Superconducting Maxwell Pair Gradient Coil Set.  $I_p$  is Produced by a Current Source Driver Amplifier.  $V_p$  is the Voltage Across the Coil Terminals.

Figure 5 - Schematic of the Measurement Calorimeter. The Maxwell Pair Coil is Placed Within the Inner Shield, and is Represented by the Equivalent Circuit  $L_{ext}$ ,  $L_{int}$ ,  $R_H$ ,  $G$ , and  $R_{Series}$ . Heat Can Only Flow Through the Thermal Link Between the Inner and Outer Shields. For Higher Power Dissipation Measurements, Helium Transfer Gas is Admitted Into the Inner Container.

Figure 6 - Determining the Effective Inductance for Various Wire Geometries and Sizes. The Impedance Magnitude  $|Z|$  vs Frequency is Measured. Inductance is Derived as  $|Z|/\omega$ .

Figure 7 - Illustrating the Frequency Dependence of a 1 Turn Coil. Distinct Regions, Corresponding to the AC Resistance Increasing as  $f$  (hysteresis) or  $f^2$  (inductive-Ohmic) Rates, are Shown.

Figure 8 - Data for Three Different Types of Superconducting Cable Described in the Text. Effect of Number of Turns, Inductance, and Wire Cross-sectional Area on AC Loss Resistance  $R_{ac}$ .

Figure 9 - Effect of Temperature on  $R_{ac}$ . A Four Turn Coil is Measured at  $8^{\circ}$  and  $12^{\circ}$  K.

Figure 10 - Dependence of AC Power Dissipation on Externally Applied Magnetic Field  $B_0$

Figure 11 - The Dependence of the Hysteresis Resistance on AC Drive Current. Note:  $R_{ac}$  is of the form  $R_{HO} f + (\omega L)^2 G$ , and  $R_{HO} = R_{HO}^{(small)} \{1 + 0.68 (I_p/I_c)^2 + 20.5 (I_p/I_c)^4 + \dots\}$ .

Figure A-1 - Timing Relationships in Echo Planar Imaging and Definitions for the Gradient Waveform.

Figure B-1 - Plot of the B vs H Constitutive Relation for a Hypothetical Superconductor with Transition Temperature  $T_c = 18^{\circ}$  K, and Operating Temperatures T of 1, 8, or  $18^{\circ}$  K. Also Illustrated is the Relationship  $B = \mu H$  for a Normal Metal.

Figure B-2 (a) - Superconducting Cable Internal Inductance vs. Drive Current  $I_p$ . Superconductor Operated at 8, 10, or  $12^{\circ}$  K.

Figure B-2 (b) - Superconducting Cable Internal Inductance vs. Operating Temperature.

Figure D-1 - Photograph of Gradient Coils Mounted on the Fiberglass Former with Heater Coils in Place.

Figure D-2 - Photograph of Completed Calorimetric Device, Assembled and Ready to be Placed in the Cryostat.

## Bibliography

- <sup>1</sup> L. E. Crooks, L Kaufman, Magnetic Resonance Imaging of the Body, Raven Press, New York, 1987, Chapters 1 & 2. Edited by C. B. Higgins and H. Hricak
- <sup>2</sup> P. Mansfield, P.G. Morris, NMR Imaging in Biomedicine, Academic Press, New York, 1982, Chapters 3 and 8. (An excellent primer on the major design problems faced in MRI scanners)
- <sup>3</sup> M. K. Stehling, R. Turner, P. Mansfield, "Echo-Planar Imaging: Magnetic Resonance Imaging in a Fraction of a Second," *Science*, vol. 254, pp.43-50, 4 October 1991.
- <sup>4</sup> M. S. Cohen, R. M. Weisskopf, "Ultrafast Imaging," *Magn. Reson. in Med.*, vol. 9, 1991, pp. 1-37.
- <sup>5</sup> F. W. Wehrli, Fast Scan Magnetic Resonance, Raven Press, New York, 1991, Chapters 2 and 10.
- <sup>6</sup> C. H. Meyer, B. S. Hu, D. G. Nishimura, A. Macovski, "Fast Spiral Coronary Artery Imaging," *Magn. Reson. Med.*, vol. 28, 202-213, 1992.
- <sup>7</sup> M. P. Maley, J. D. Thompson, L. R. Newkirk, "AC Losses in Nb<sub>3</sub>Ge Composite Tape Conductors," *Cryogenics*, vol. 21, no. 11, pp.675-678, Nov. 1981.
- <sup>8</sup> C. Kittel, Introduction to Solid State Physics, 3rd Edition , pp.335 - 343, John Wiley, New York, 1966
- <sup>9</sup> A. C. Rose-Innes, E. H. Broderick, Introduction to Superconductivity, Second Edition, Pergamon Press, Oxford, UK., 1978.
- <sup>10</sup> P. H. Melville, "A.C. Loss and Related Effects in Type II Superconductors," *Adv. Phys.*, vol. 21, no.92, July 1972, pp.647 - 689.
- <sup>11</sup> P. H. Melville, "Theory of ac loss in type II superconductors in the Meissner state," *J. Phys. C:Solid St. Phys.* vol.4, 1972, pp.2833-2848.
- <sup>12</sup> W. T. Norris, "Calculation of Hysteresis Losses in Hard Superconductors Carrying AC: Isolated Conductors and Edges of Thin Sheets," *J. Phys. D: Appl. Physics*, vol. 3, 1970, pp. 489-507.
- <sup>13</sup> For example, Cryomech Co., model GB37 cryo-refrigerator, Syracuse, NY,13210
- <sup>14</sup> P.A. Bottomley, "A Versatile Magnetic Field Gradient Control System for NMR Imaging," *J. Physics E14*, 1981, pg. 1081.
- <sup>15</sup> R. Turner, "Minimum Inductance Coils," *J. Physics E: Sci. Instrum.*, vol. 21, 1988, pp. 948-952.
- <sup>16</sup> S. Pissanetzky, "Minimum Energy MRI Gradient Coils of General Geometry," *Measure. Sci. Technology* vol. 3, pp. 667-673, 1992. Published in the U.K. by IOP Publishing, London.
- <sup>17</sup> P. Webb, H-P Laboratories, Palo Alto, CA., private communication.
- <sup>18</sup> J. A. Good, Properties of High Field Superconductors, D. Phil. Thesis, Oxford University, 1969.
- <sup>19</sup> K. N. Mirchandani, K. K. Das, B. Kumar, "AC Losses in Y<sub>1</sub>Ba<sub>2</sub>Cu<sub>3</sub>O<sub>7-δ</sub>:Ag Tapes," *J. of Superconductivity*, vol.6, No.6, 1993.
- <sup>20</sup> J. Lopez, "Cryostat" - a LabVIEW Automatic Measurement System, Final Report, H-P Laboratories, September 28, 1994, Palo Alto, CA.

<sup>21</sup> F. W. Grover, Inductance Calculations, Working Formulas and Tables, Dover Publications, New York, N.Y., 1973.

<sup>22</sup> S. Ramo, J. R. Whinnery, Fields and Waves in Modern Radio, Second Edition, John Wiley and Sons, New York, 1962, pp.258 - 262.

<sup>23</sup> J. A. Eikelboom, "Test results of an Apparatus for Calorimetric Measurement of AC Losses in Superconductors," IEEE Trans. on Magnetics, vol. 28, no. 1 , pp. 817-821, Jan. 1992.

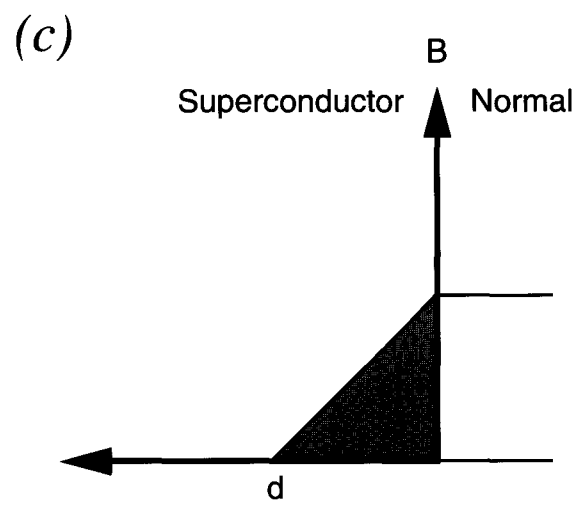
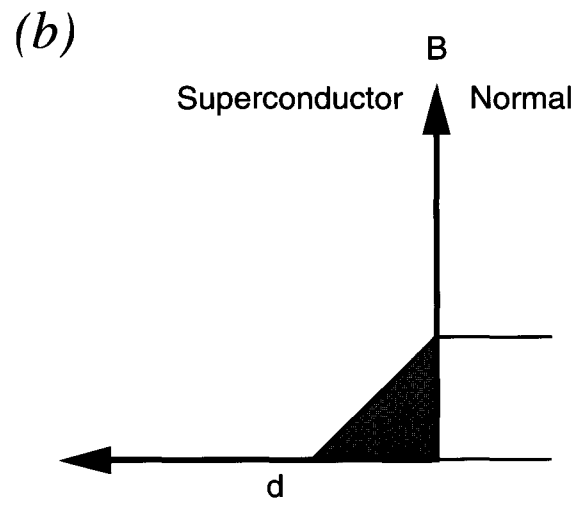
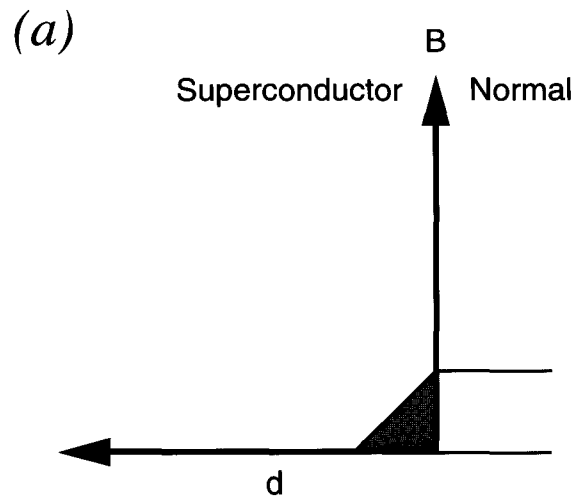


**Figure 1**

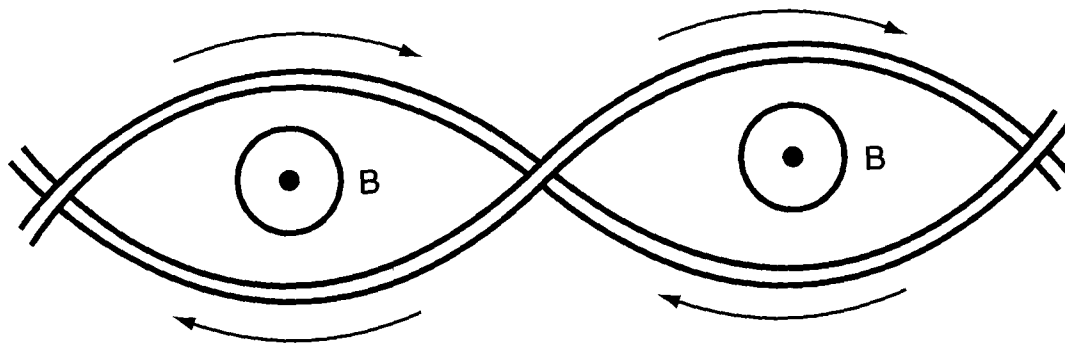


**Figure 2**

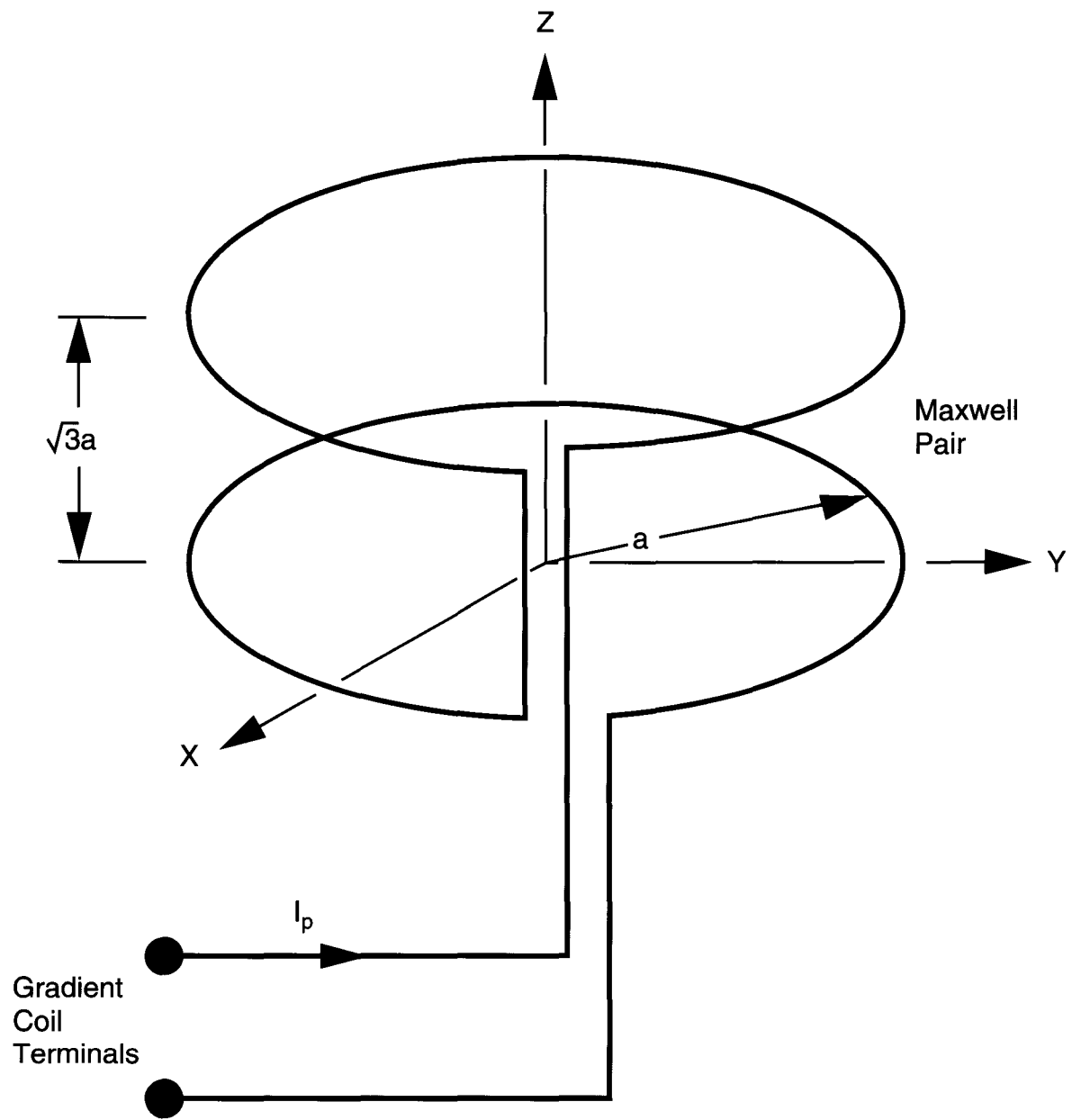


**Figure 3**

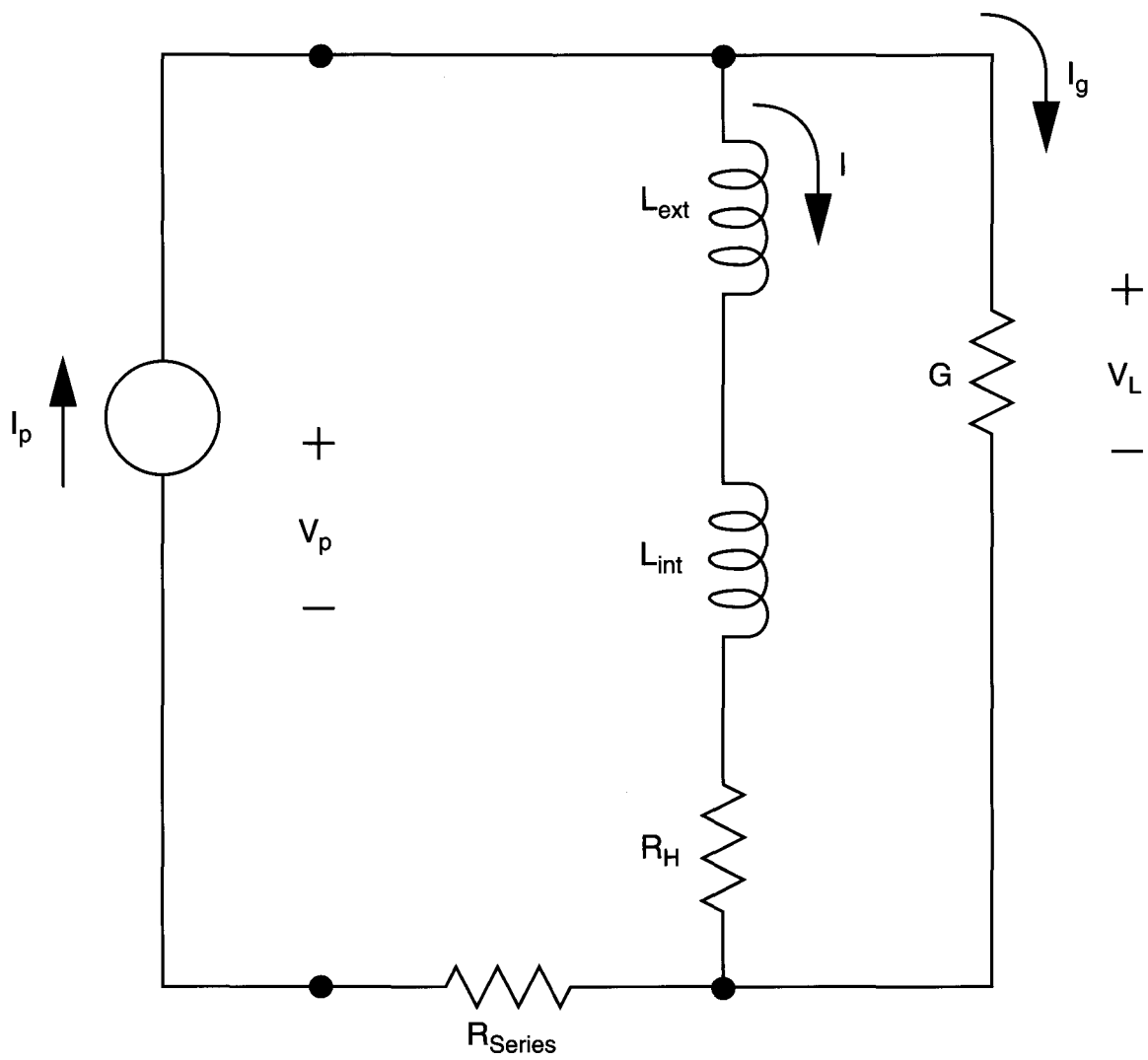


**Figure 4**

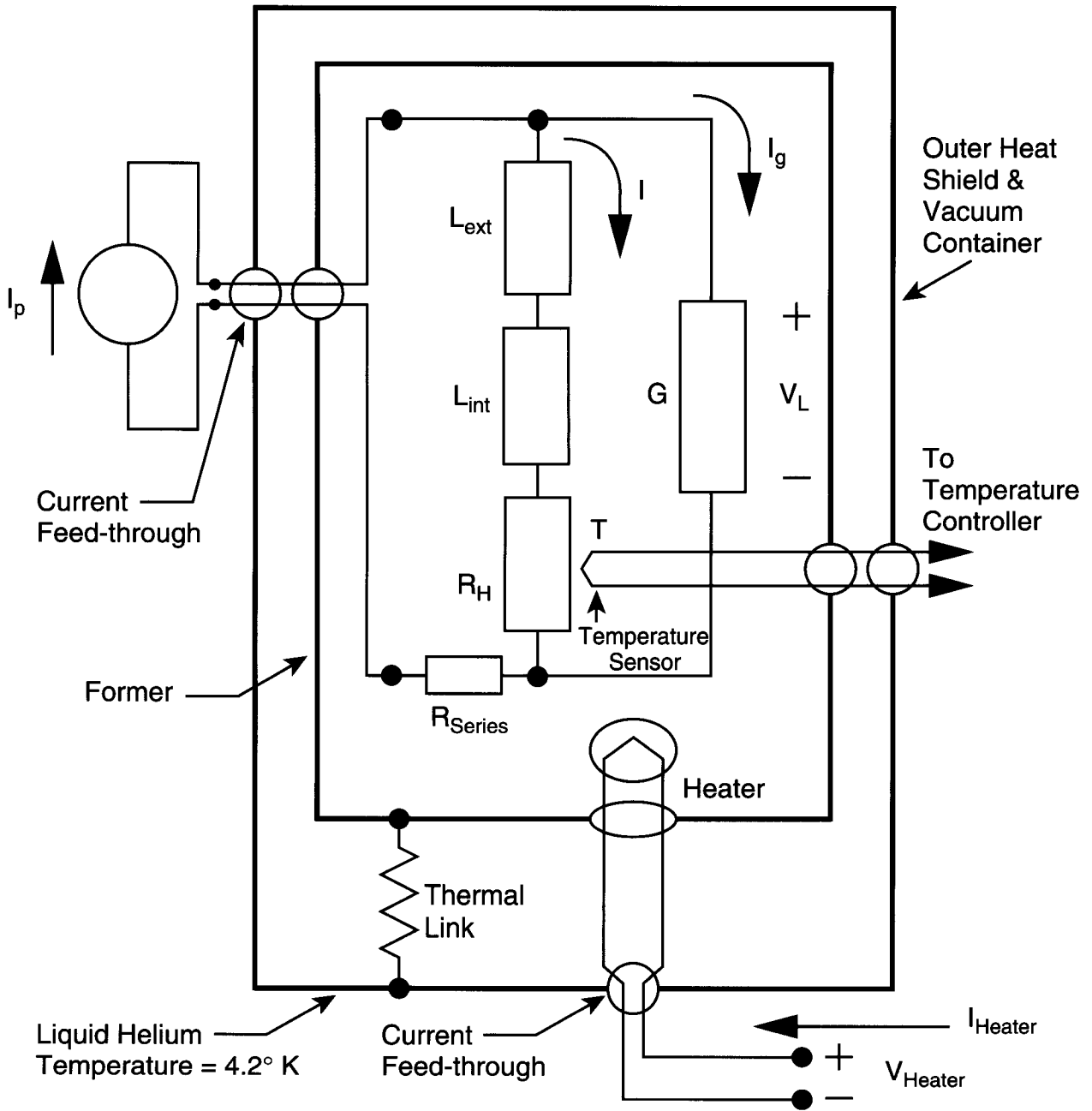


Figure 5

Parameters: various wire diameters,  
 100 mm loop diameter  
 Temperature = 8° K     $B_0 = 0$  Tesla  
 Drive current  $I_p = 20$  Amps

- ◇ ± 4 turn coil, 0.4 mm wire,             $L = 8.162 \mu\text{H}$
- ◊ ± 1 turn coil, 0.4 mm wire,             $L = 0.940 \mu\text{H}$
- ± 1 turn coil, 1.1 mm wire,             $L = 0.795 \mu\text{H}$
- ± 1 turn coil,  
 6 strand Rutherford coil,  
 0.4 mm wire                                 $L = 0.678 \mu\text{H}$

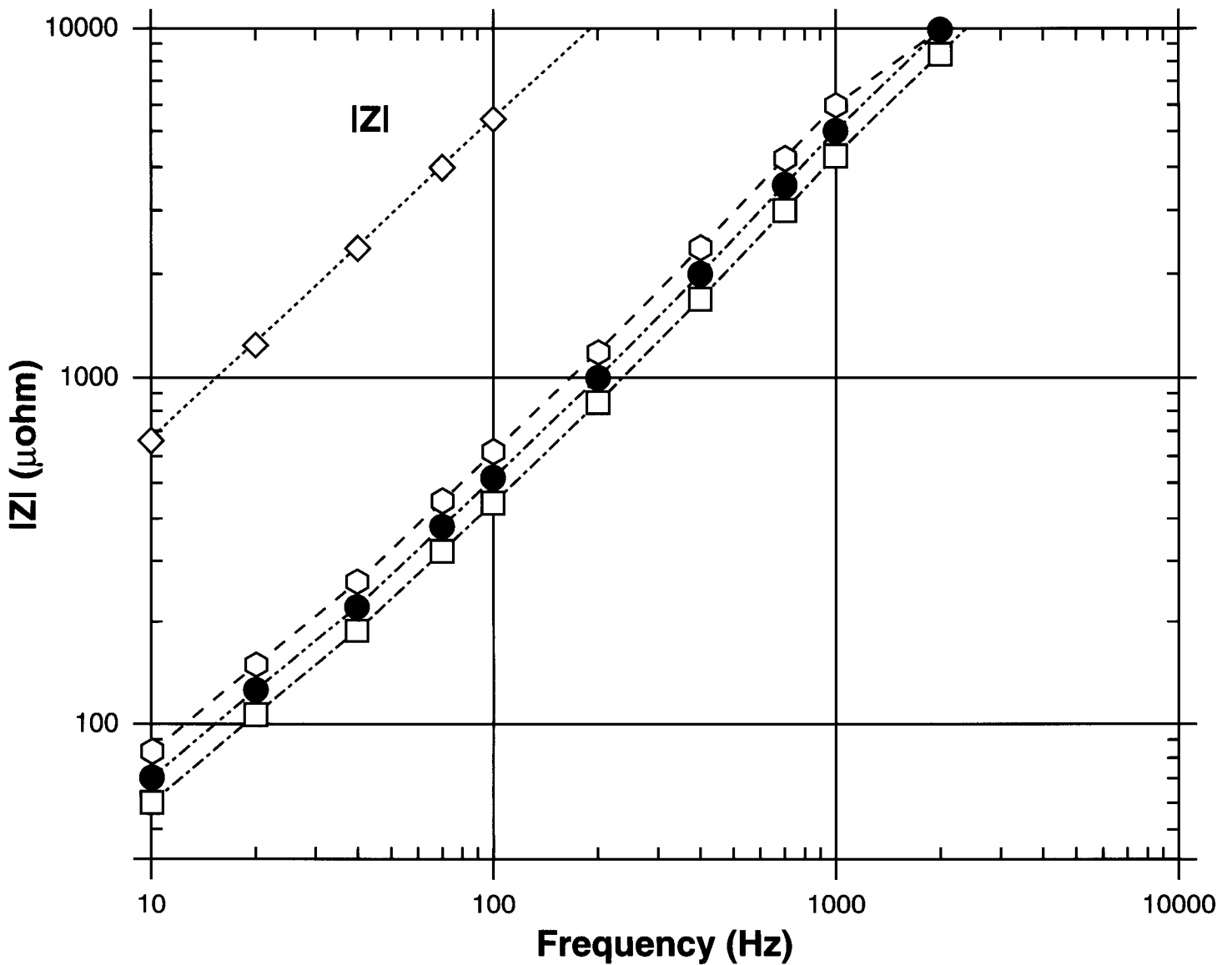


Figure 6

Parameters:  $\pm 1$  turn coil, 1.1 mm wire diameter,  
100 mm loop diameter

Temperature =  $8^\circ$  K       $B_0 = 0$  Tesla

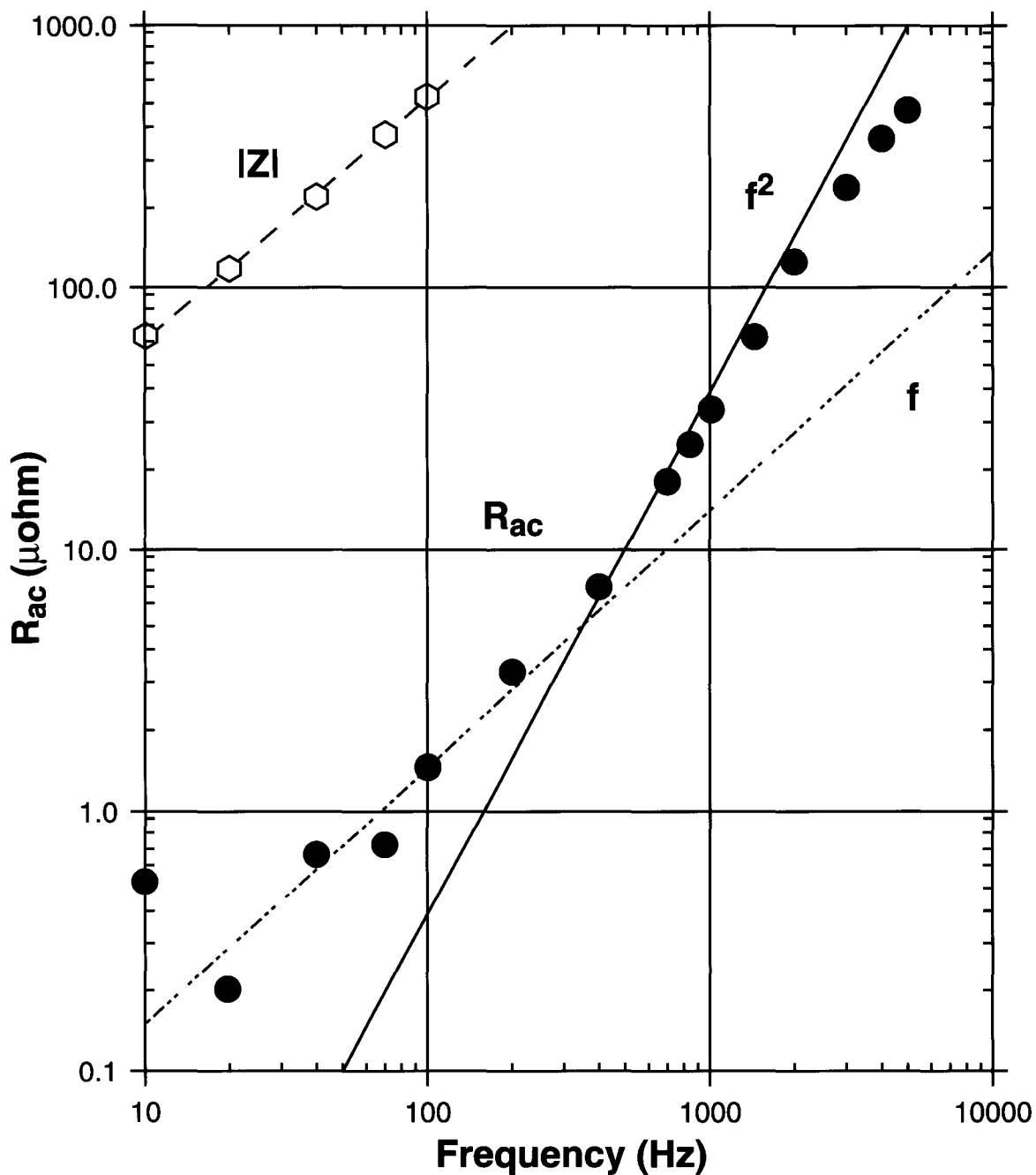
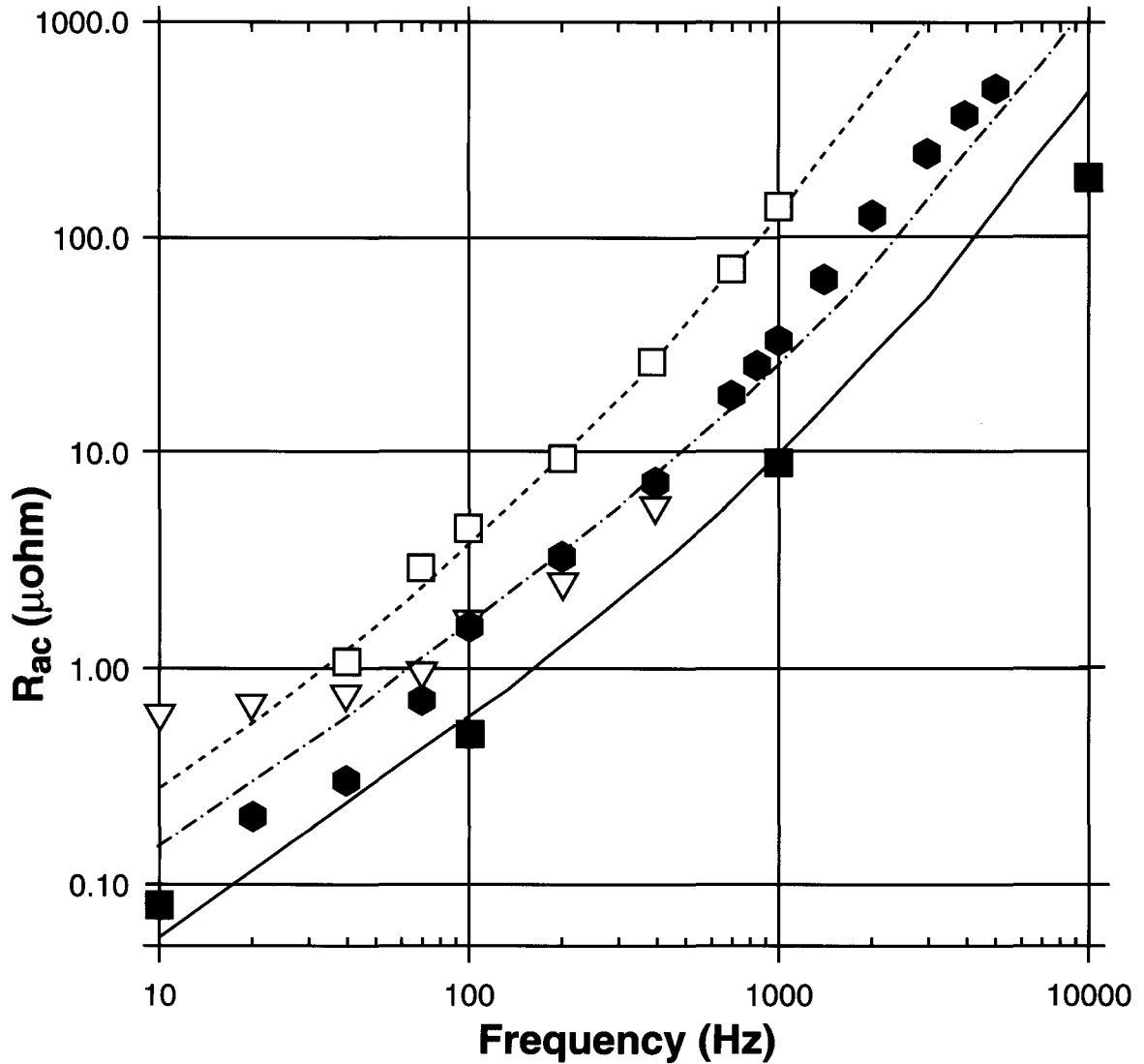


Figure 7

Parameters:  $\pm 1$  turn coil or  $\pm 4$  turn coil  
 Temperature =  $8^\circ\text{K}$   $B_0 = 0$  Tesla  
 Drive current  $I_p = 30$  Amps

- $\pm 1$  turn coil, 0.4 mm wire (old)
- $\pm 4$  turn coil, 0.4 mm wire (old)
- ▽  $\pm 1$  turn coil, 0.4 mm wire (new)
- $\pm 1$  turn coil, 1.1 mm wire (copper core)



- 1 turn coil, old 0.4 mm wire - theory
- - - 1 turn coil, new 0.4 mm wire - theory
- · · 4 turn coil, old 0.4 mm wire - theory

Figure 8

Parameters:  $\pm 4$  turn coil, 0.4 mm wire (old),  
100 mm loop diameter  
Temperature =  $8^\circ\text{K}$  or  $12^\circ\text{K}$   $B_0 = 0$  Tesla  
Drive current  $I_p = 20$  Amps

○  $R_{ac}$  at  $8^\circ\text{K}$   
●  $R_{ac}$  at  $12^\circ\text{K}$

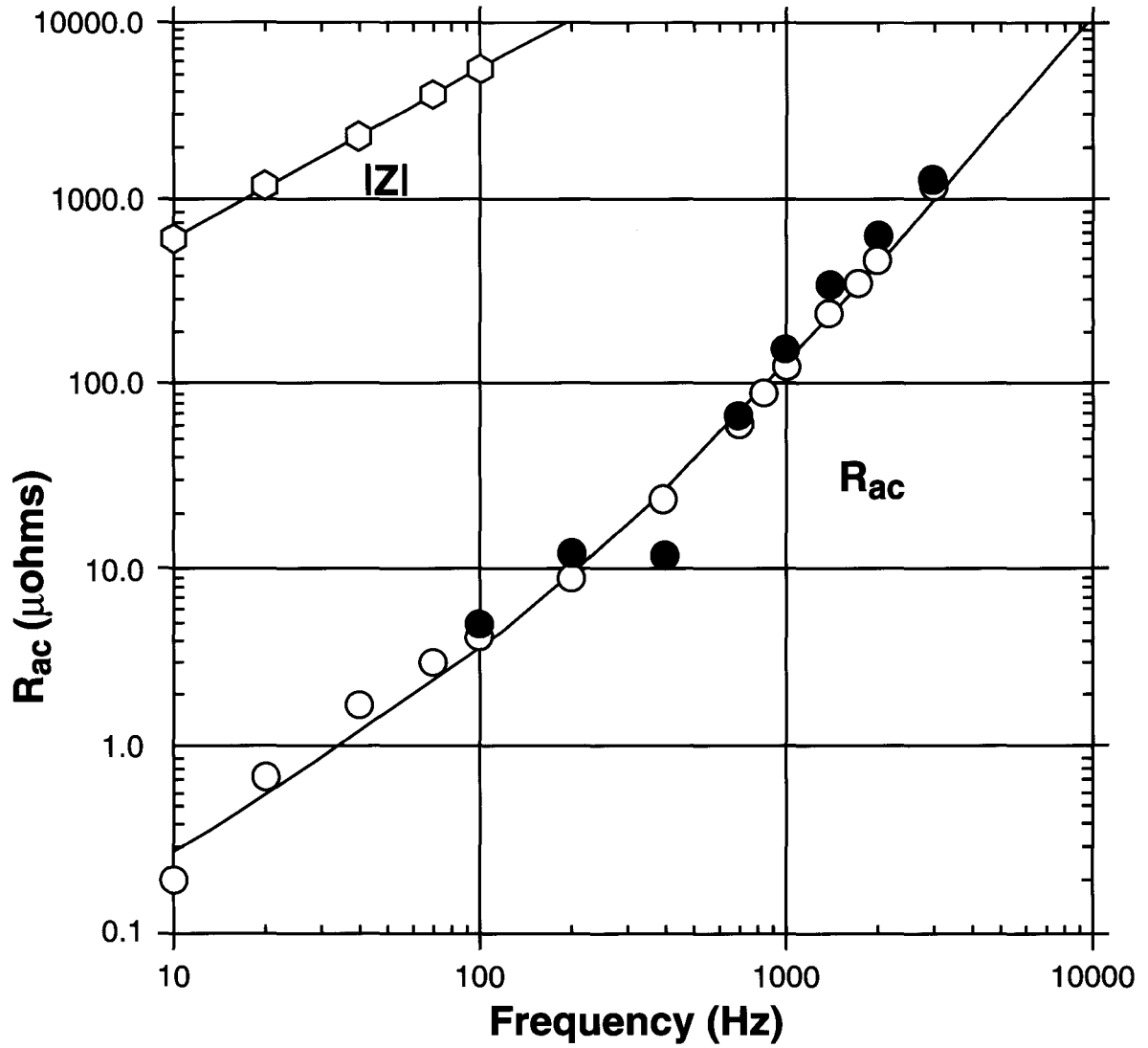
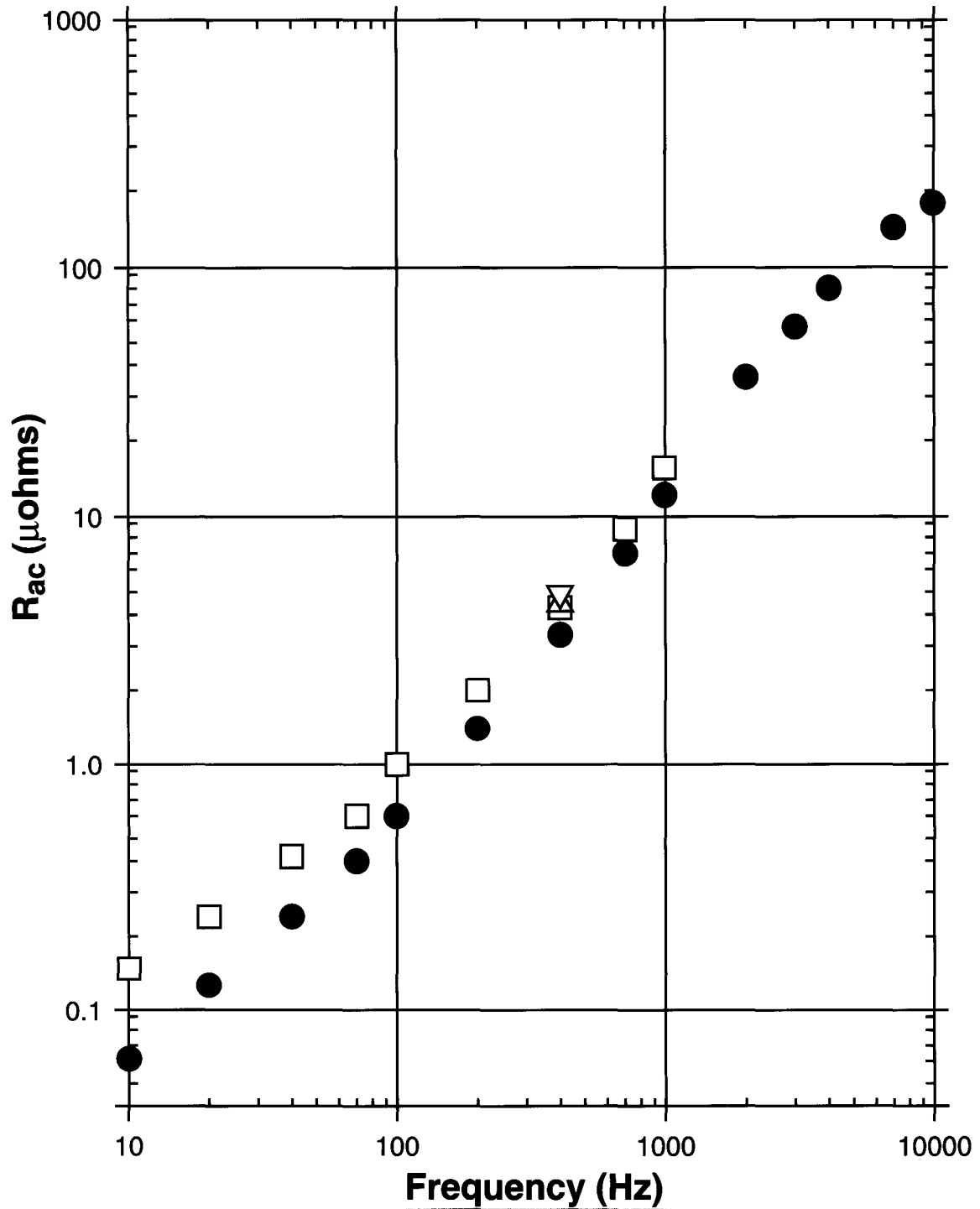


Figure 9

**Parameters:  $\pm 1$  turn coil, 0.4 mm wire (old),  
100 mm loop diameter  
Temperature = 8° K**

**Applied DC Magnetic Flux Density  
 $B_0$  (Tesla)**

- 0 Tesla
- △ 1.0 Tesla
- 0.5 Tesla
- ▽ 1.5 Tesla



**Figure 10**

**Measured Data (points) and Fit (line) to Theory of Appendix B**  
**Temperature:  $T_c = 18^\circ \text{ K}$ ,  $T = 8^\circ \text{ K}$ ,  $B_0 = 0 \text{ Tesla}$**

- $\pm 1$  turn coil, 0.4 mm wire (new)
- Fitted line

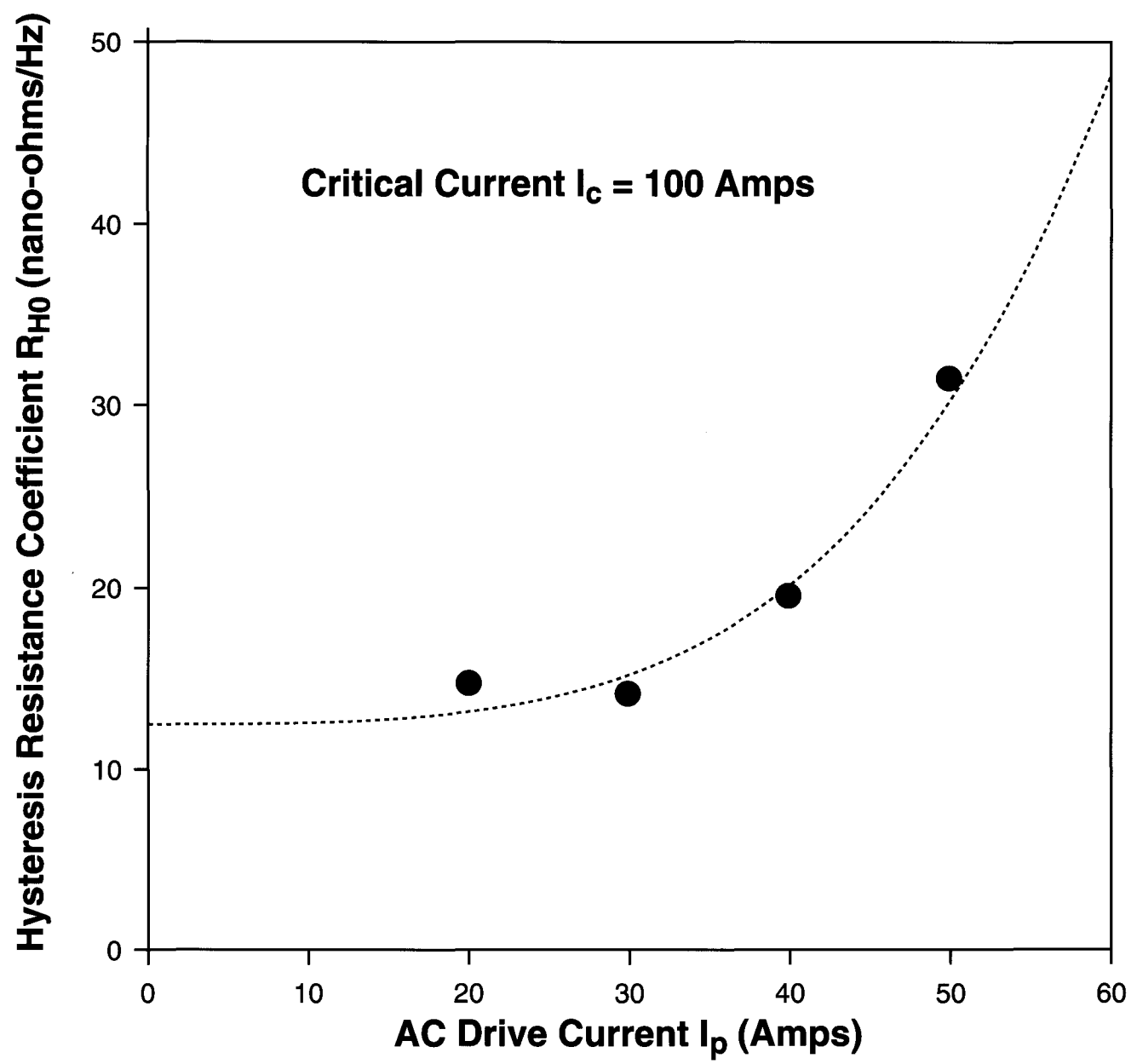


**Figure 11**

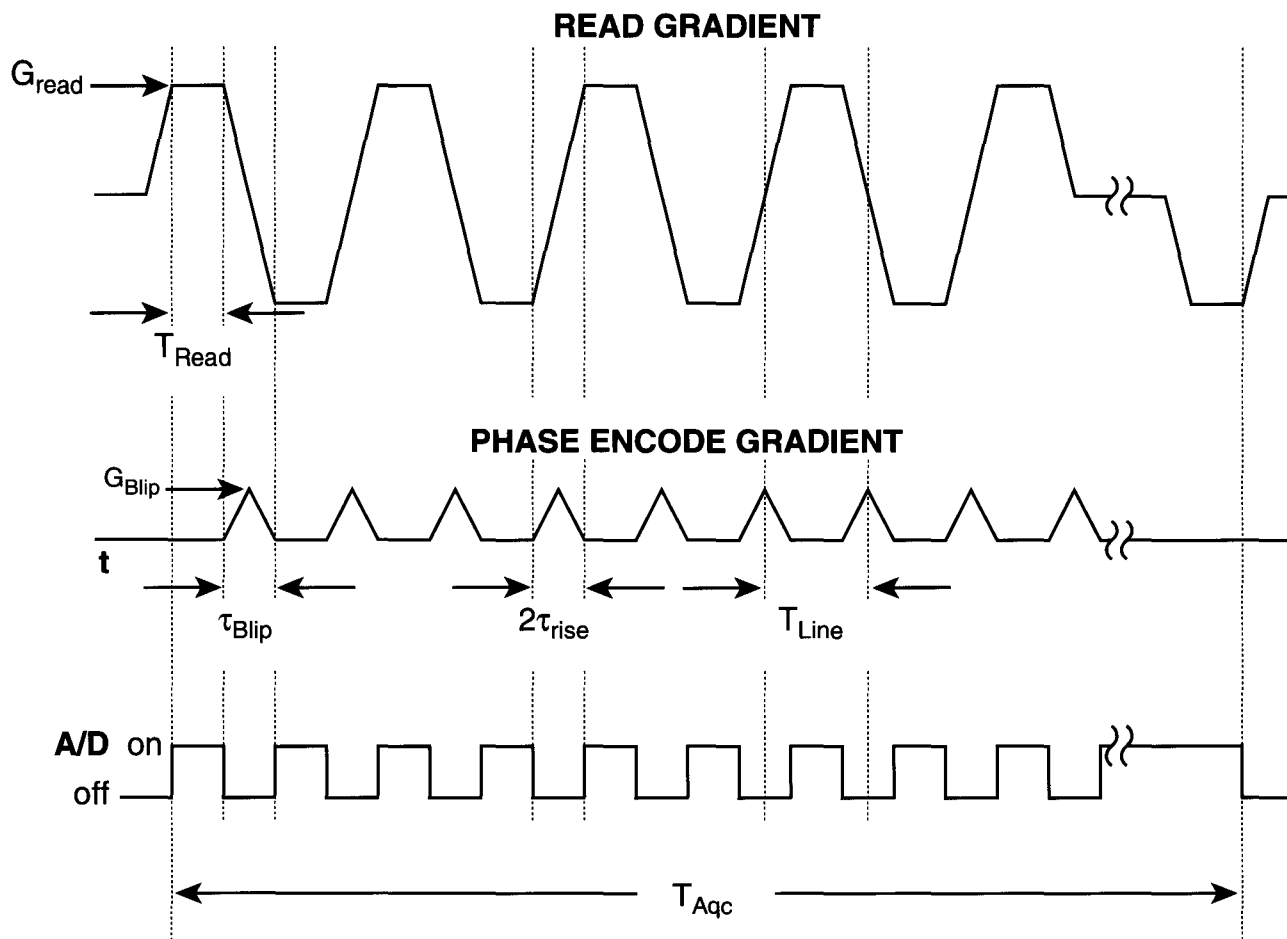


**Figure A-1**

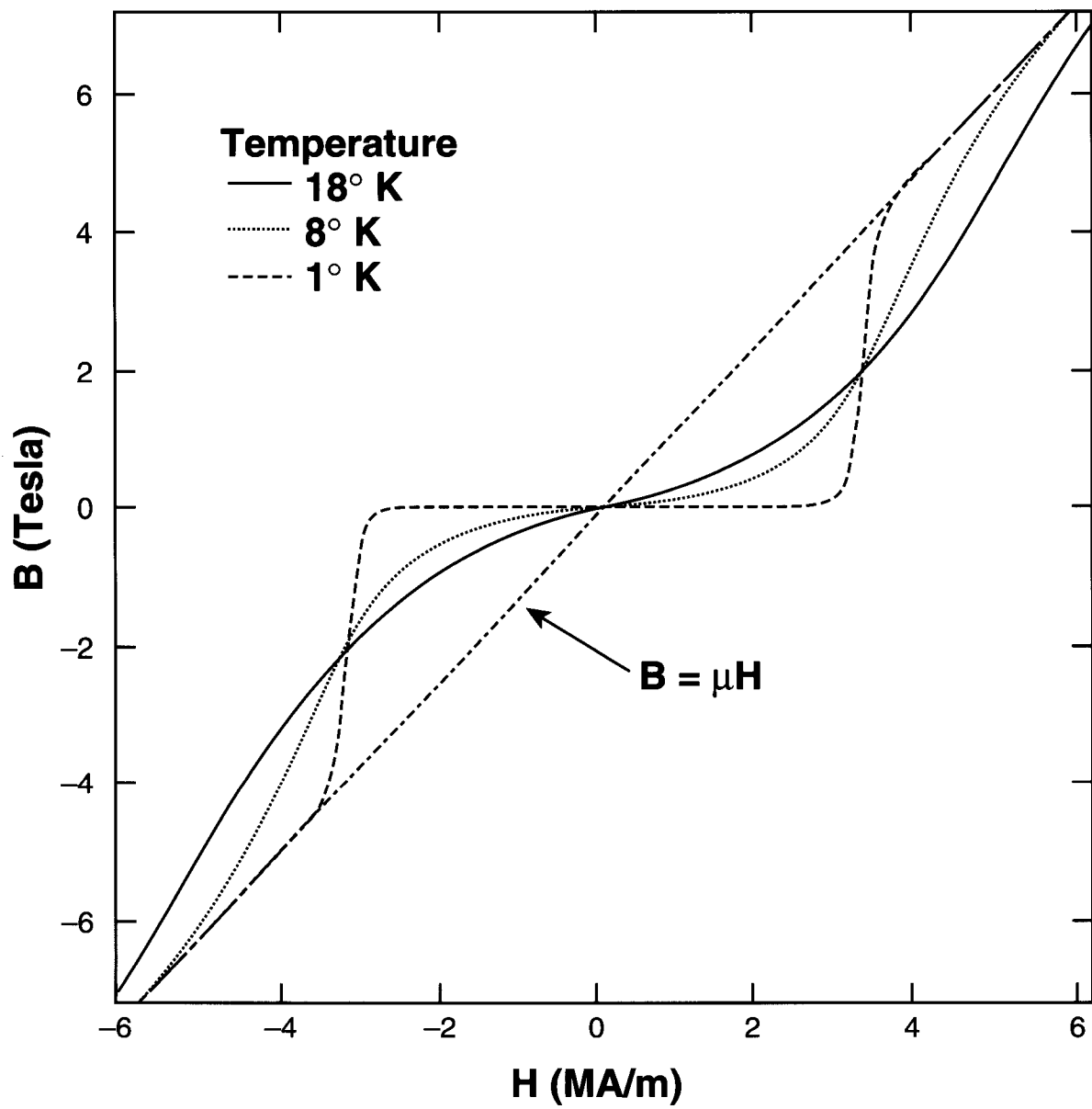


Figure B-1

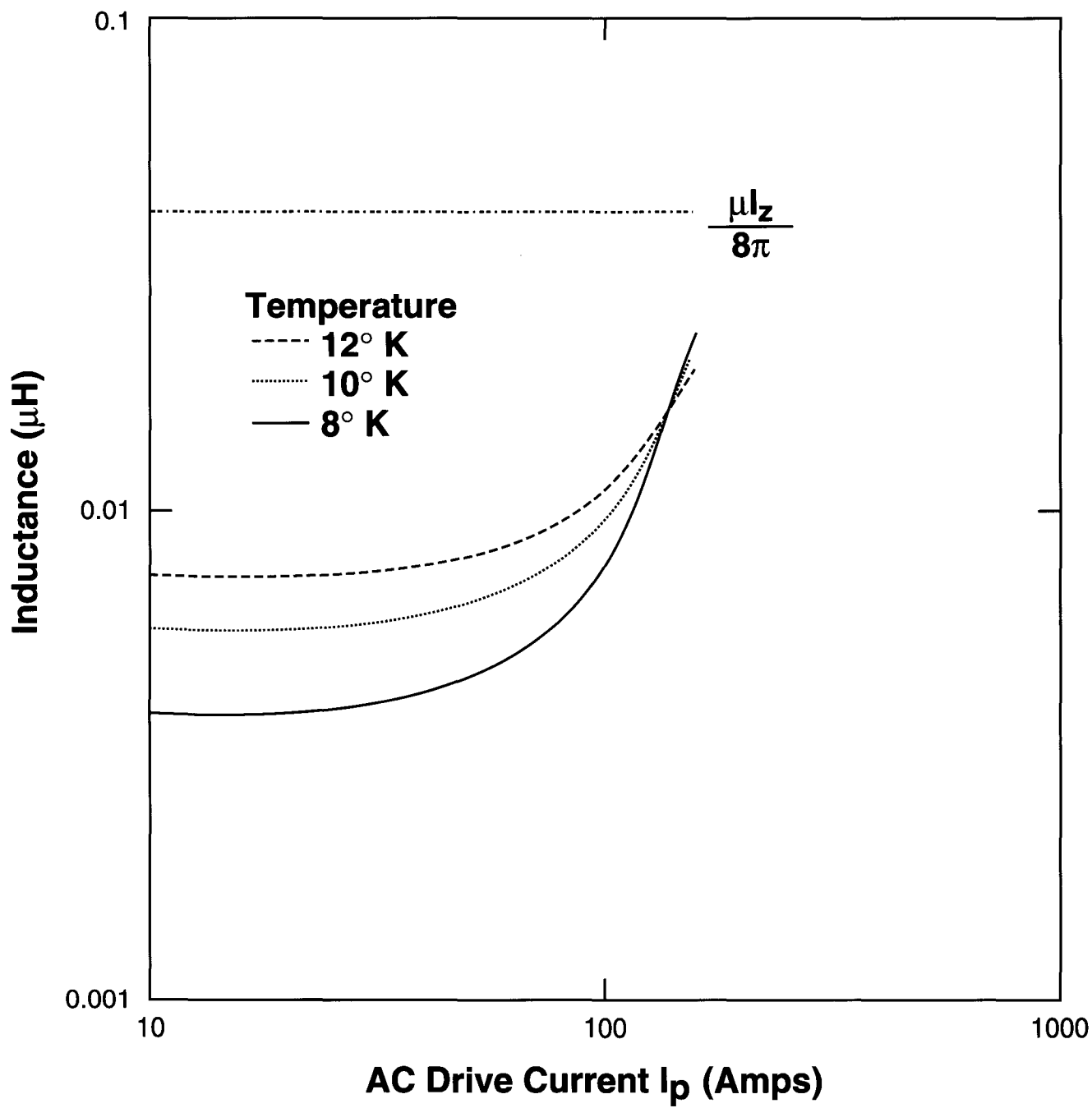


Figure B-2 (a)

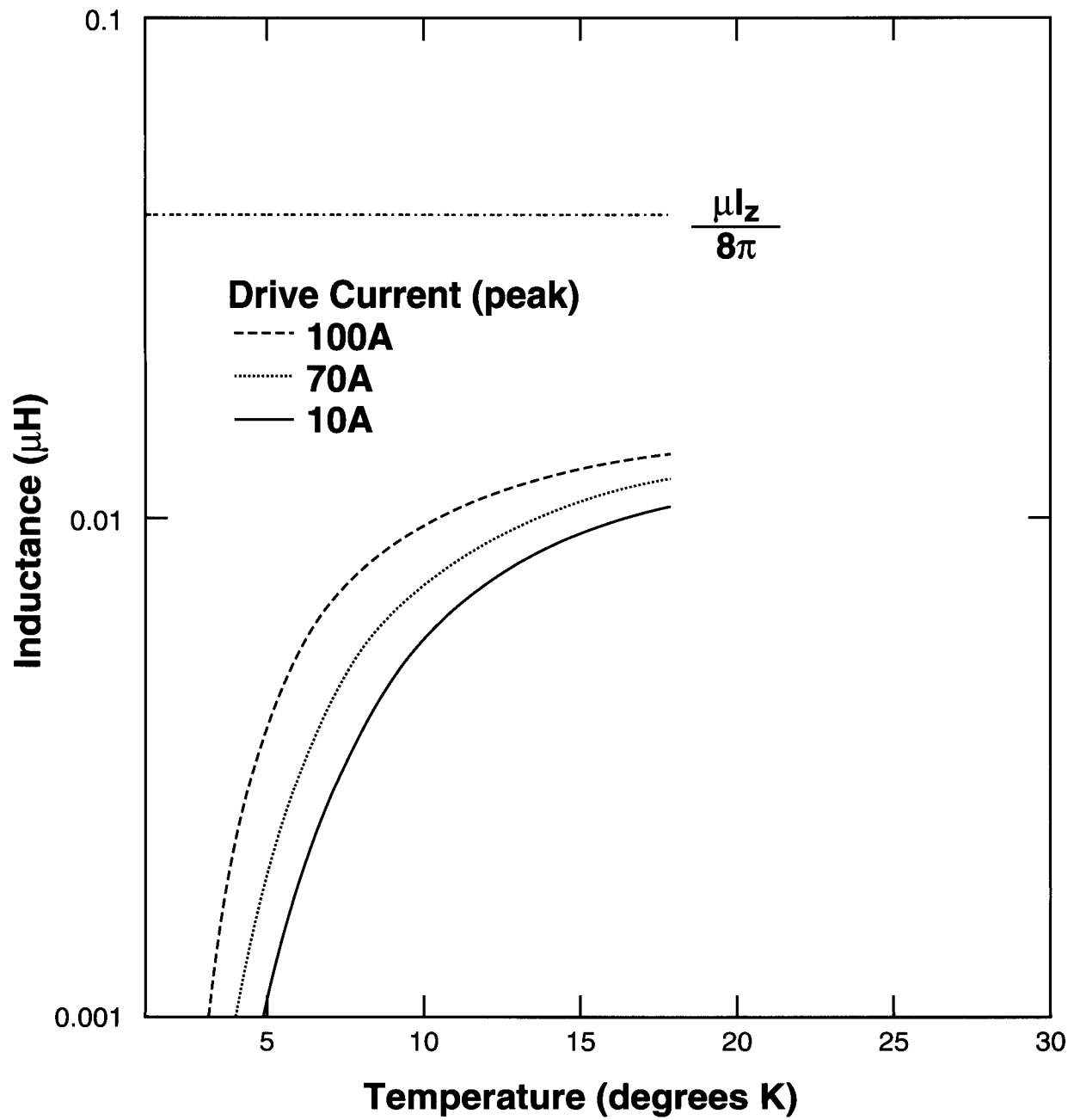
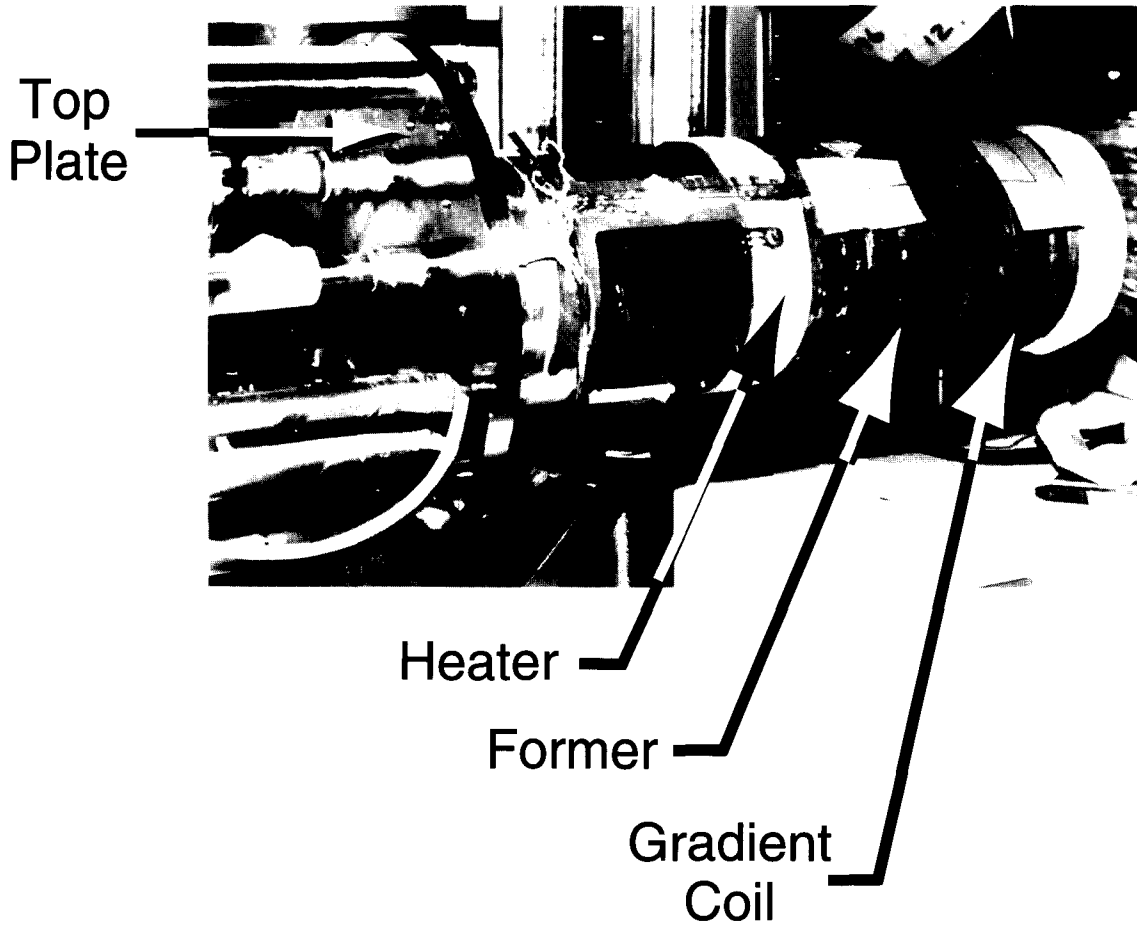
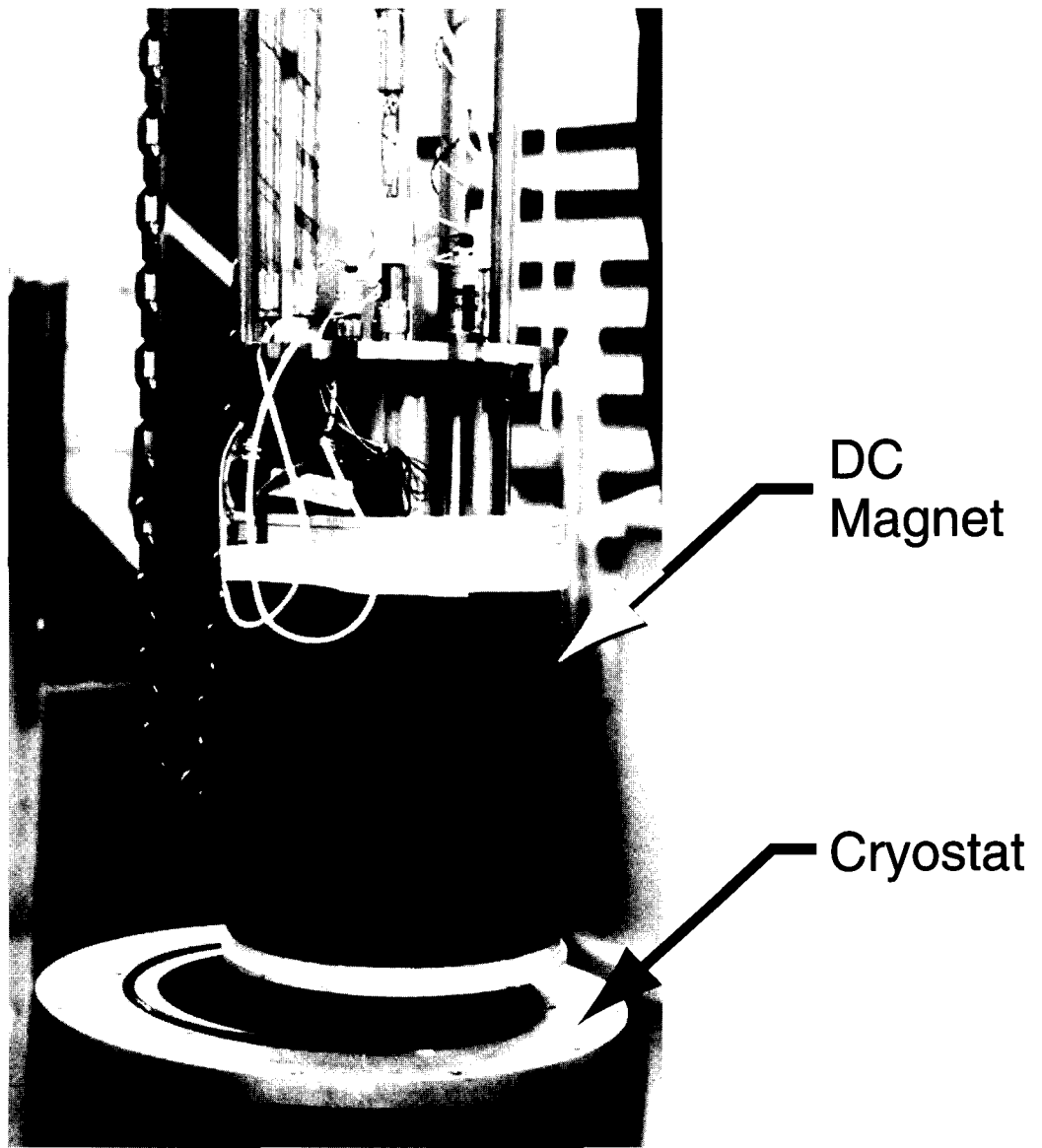


Figure B-2 (b)



**Figure D-1**



**Figure D-2**